published in *Scale Invariance, Interfaces, and Non-Equilibrium Dynamics*, edited by A. J. McKane, M. Droz, J. Vannimenus, and D. E. Wolf, NATO ASI Series B, Vol. 344 (Plenum, New York, 1995), pp. 165-202.

NON-EQUILIBRIUM ORDERING DYNAMICS AND PATTERN FORMATION

Martin Siegert

Theoretische Physik, FB10
Gerhard-Mercator-Universität Duisburg
47048 Duisburg
Germany

1. INTRODUCTION

When a system is quenched from a disordered homogeneous high temperature phase into a low-temperature regime, where several phases coexist, a complex domain structure develops. As time proceeds this domain structure coarsens and the average radius of the domains grows. The late stages of this phase ordering process is believed to show universal scaling behavior: It is found that the kinetics are dominated by a single length scale, the domain size $R(t)$, which increases with a power law in time, $R(t) \sim t^{1/z}$. This fact is illustrated in Fig. 1. The domain patterns a)-c) belong to three different times. But if the graphs are rescaled by the domain size, indicated in the figures, quite similar pictures are obtained. Thus, the pictures at later times look like enlargements of the early time configurations. The exponent z depends on the conservation laws governing the dynamics and the dimension n of the order parameter, but not on the microscopic details of the system. Although some of the classic papers[1−3] on the kinetics of first-order phase transitions and domain growth have been published more than 30 years ago there has recently been a renewed interest in the theory of phase ordering, especially due to the interest in systems with a vector order parameter. In this article I will give an overview of these new developments.

As an introduction I will review in the first section the Allen-Cahn theory[1] for a nonconserved scalar order parameter and the Lifshitz-Slyozov-Wagner theory[2,3] for a conserved scalar order parameter. In the main part the newer theories of phase ordering will be presented and their predictions will be compared with the results of numerical simulations. Finally, in the last section the pattern formation of growing surfaces in molecular beam epitaxy and its relation to domain growth phenomena will be discussed.

Throughout this paper I will use magnetic language, i.e., the order parameter is

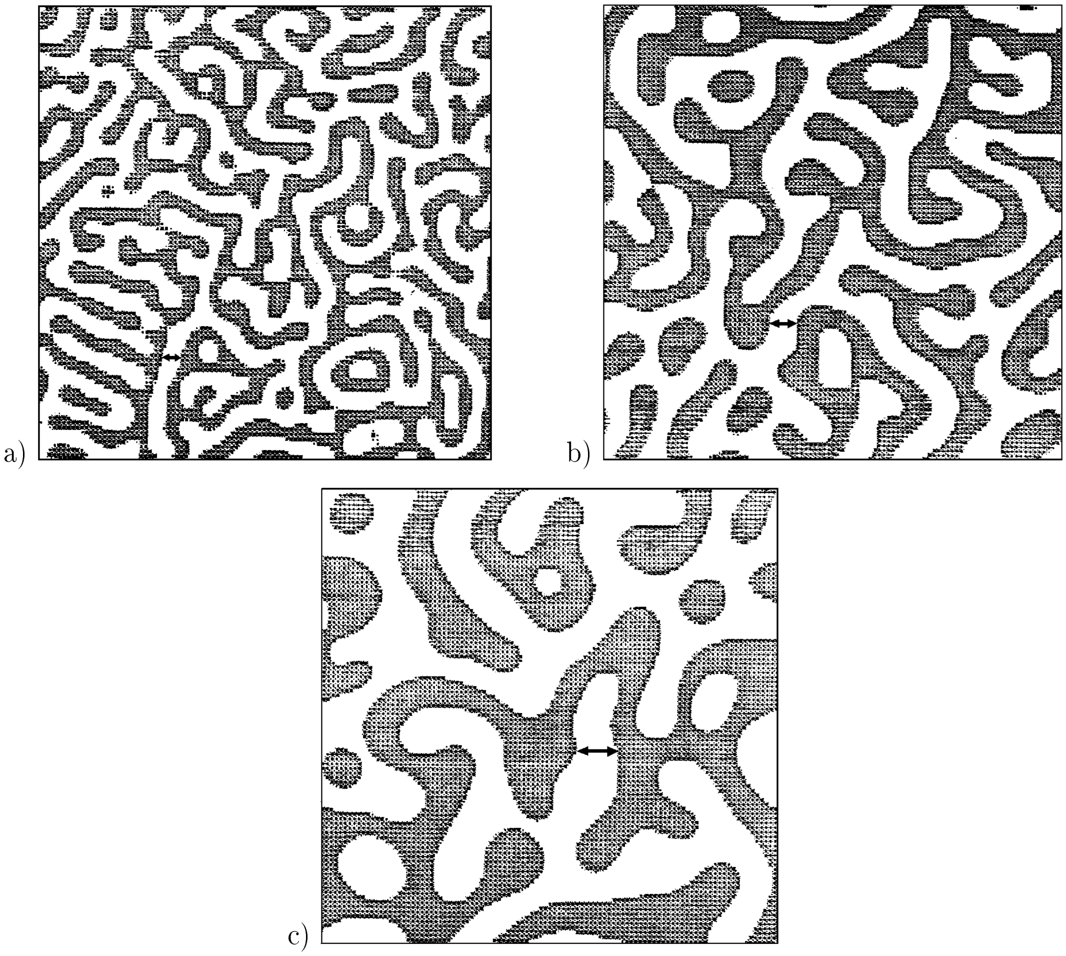

Figure 1. Domain growth for a conserved scalar order parameter, time increases from a) to c). The typical lengthscale, $R(t)$, is indicated by an arrow. The configurations were generated by a numerical integration of Eq. (2.19) (From T. M. Rogers, K. R. Elder, and R. C. Desai, Phys. Rev. B **37**, 9638 (1988), reprint kindly permitted by the authors).

called magnetization, although the same phenomenon occurs in many other systems, e.g., for a conserved scalar order parameter in binary alloys, where the phenomenon is known as Ostwald ripening, or in fluids, where it is called spinodal decomposition.

2. THE CLASSICAL THEORIES

2.1 Nonconserved Order Parameter

First, the dynamical theory of Allen and Cahn[1] for a nonconserved scalar order parameter will be revisited. Let us consider an Ising-like system described by a Ginzburg-Landau free energy functional

$$\mathcal{F}[\Phi] = \int d^d x \left[\tfrac{1}{2} c (\nabla\Phi)^2 + V(\Phi)\right] \ , \tag{2.1}$$

where $\Phi(\mathbf{x}, t)$ is the local order parameter and the potential $V(\Phi)$ has two degenerate minima at $\Phi = \pm\Phi_0$. The domain wall profile of a flat equilibrium interface is determined by the minimum of the free energy, i.e, $\delta\mathcal{F}/\delta\Phi = 0$, resp.,

$$c\frac{\partial^2\Phi}{\partial x_1^2} = V'(\Phi) \tag{2.2}$$

together with the boundary conditions $\Phi(x_1 = \pm\infty) = \pm\Phi_0$. Here, x_1 is the coordinate running normal to the interface, $x_1 = 0$ being the position of the domain wall defined through $\Phi(x_1) = 0$. From (2.2) it follows that $V(\Phi) - V(\Phi_0) = \frac{1}{2}c(\partial\Phi/\partial x_1)^2$, which can be used in (2.1) to obtain the surface tension ($\equiv$ excess free energy per area of the interface, $\sigma = (\mathcal{F}[\Phi] - \mathcal{F}[\Phi_0])/A$ with Φ from (2.2))

$$\sigma = c\int_{-\infty}^{\infty} dx_1 \left(\partial\Phi/\partial x_1\right)^2 \ . \tag{2.3}$$

Note that Eq. (2.3) is not an universal relation between the surface tension and the order parameter profile. If, e.g., terms like $(\nabla^2\Phi)^2$ are included in the free energy functional (2.1) the relation (2.3) is no longer valid.

Now we will concentrate on the dynamics of a domain of plus spins in a sea of minus spins. The evolution of the order parameter is given by the Langevin equation

$$\partial_t\Phi = -\lambda'\frac{\delta\mathcal{F}[\Phi]}{\delta\Phi} + \zeta = \lambda'\left[c\nabla^2\Phi - V'(\Phi)\right] + \zeta \ , \tag{2.4}$$

where λ' is a dynamical coefficient and the noise ζ obeys the fluctuation-dissipation theorem

$$\langle\zeta(\mathbf{x},t)\rangle = 0 \quad \text{and} \quad \langle\zeta(\mathbf{x},t)\zeta(\mathbf{x}',t')\rangle = 2k_BT\lambda'\delta(\mathbf{x}-\mathbf{x}')\delta(t-t') \ .$$

In the context of critical dynamics Eq. (2.4) is equivalent to model A in the classification of Hohenberg and Halperin[4]. The Langevin equation (2.4) is most conveniently studied using normal coordinates introduced by Zia[5]. These curvilinear coordinates u_i, $i = 1,\ldots,d$, are defined through

$$\mathbf{x} = \mathbf{x}_s(\mathbf{v},t) + u_1\mathbf{n}(\mathbf{v},t) \ , \ \mathbf{v} \equiv (u_2,\ldots,u_d) \ . \tag{2.5}$$

Here, $\mathbf{n}$ is the unit vector normal to the interface and $\mathbf{x}_s$ is a vector pointing to a point on the interface. Thus, u_1 is the coordinate running normal to the domain wall, whereas the other coordinates, represented through the $d-1$ dimensional vector $\mathbf{v}$, lie in the interface. The position of the domain wall is given by $u_1 = 0$. A sketch of the coordinate system is found in Fig. 2. The coordinate system (2.5) has singularities when u_1 is of the order of the radius of curvature of the domain boundary[5]. However, we

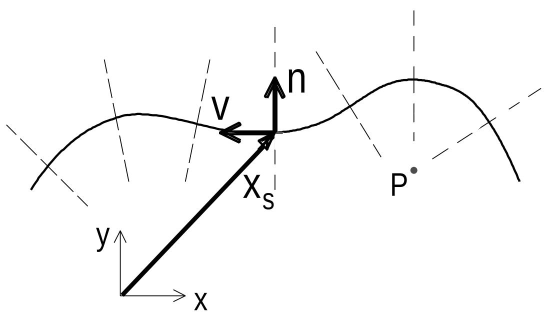

Figure 2. Normal coordinates as defined by (2.5). The solid line shows the position of the interface $u_1 = 0$. The dashed lines correspond to $\mathbf{v} = const.$ The point labelled P indicates a singularity of the coordinate system.

may assume that after an initial transient regime well defined domains of the bulk order parameter $\pm\Phi_0$ have been formed. Furthermore, if the local magnetization is suitably coarse grained so that the width of the domain walls is much smaller than the typical radius of curvature of the domain boundary then the aforementioned singularities are far away from the region of interest. Under these circumstances we may approximate the order parameter profile Φ by the profile of the flat interface resulting from (2.2) with x_1 replaced by $u_1(t)$. Thus, using (2.2) in (2.4) we obtain

$$\partial_t u_1 \frac{\partial \Phi}{\partial u_1} = -\lambda' c \kappa \frac{\partial \Phi}{\partial u_1} + \zeta \tag{2.6}$$

where

$$\kappa = -\nabla \cdot \mathbf{n} = -\nabla^2 u_1 \tag{2.7}$$

is the curvature (more accurately, the trace of the curvature tensor) of surfaces $u_1 = const$; $\kappa(u_1 = 0)$ is the curvature of the domain boundary. As mentioned above we assume that the width of the domain wall is much smaller than the radius of curvature of the domain boundary. It is therefore reasonable to regard κ and $\partial_t u_1$ as approximately constant over the width of the domain wall. Multiplying (2.6) by $\partial\Phi/\partial u_1$ and integrating over u_1 we obtain the Allen-Cahn equation[1,6,7]

$$\partial_t u_1 = -\lambda \sigma \kappa + \eta \tag{2.8}$$

that describes domain growth for a nonconserved Ising-like order parameter. The noise $\eta = -\int du_1 \left[(\partial\Phi/\partial u_1)\zeta\right]/I_0$, $I_0 = \int du_1 (\partial\Phi/\partial u_1)^2$, still obeys a fluctuation-dissipation theorem

$$\langle \eta(\mathbf{x}_s, t)\eta(\mathbf{x}'_s, t')\rangle = 2k_B T \lambda \delta(\mathbf{x} - \mathbf{x}')\delta(t - t')$$

with the kinetic coefficient

$$\lambda = \lambda'/I_0 \ . \tag{2.9}$$

Eq. (2.8) states that the local normal velocity $v = \partial_t u_1$ of the domain wall is proportional to the local curvature, and that the growth is driven by the surface tension of the domains. From (2.8) it follows immediately that a domain with an average radius $R(t)$ shrinks in time according to $R^2(t) = R^2(0) - 2\lambda(d-1)t$. Hence a droplet with an initial radius $R(0)$ has a finite lifetime $t \sim R^2(0)$. Consequently, the dynamic exponent is

$$z = 2 \tag{2.10}$$

for a nonconserved scalar order parameter.

Quite often the Allen-Cahn equation (2.8) is written without the surface tension on the right hand side since the integral I_0 drops out of the product $\lambda\sigma$ and the constant c may be scaled to 1. This cancelation is, in fact, an artefact of the approximations made: That both λ and σ are proportional to I_0 has its origin *inter alia* in the form of the free energy functional (2.1) as already mentioned above. If, e.g., lattice anisotropies are included in the calculation Eq. (2.9) remains unchanged, although in that case I_0 depends on the local orientation of the interface[8]. Consequently, the kinetic coefficient attains an angle dependence, $\lambda = \lambda(\mathbf{n})$. However, the surface tension in (2.8) has to be replaced by the surface stiffness[8] which depends on the interface orientation $\mathbf{n}$ as well. The angle dependences of the kinetic coefficient and the surface stiffness are different in general. As it stands Eq. (2.8) demonstrates that the surface tension σ and the dynamical coefficient λ are physically independent quantities.

It is instructive to compare the Allen-Cahn theory with the results for the dynamics of a pure surface model. We will see that the result (2.8) can be obtained by considering the motion of a surface driven by surface tension. The free energy functional of a surface is usually taken as that of a drumhead model

$$\mathcal{F} = \mathcal{F}_{\rm DH} = \sigma \int d^{d-1}x \, \sqrt{g} \quad \text{with} \quad g = 1 + (\nabla h)^2 \ , \tag{2.11}$$

where h is a function of the surface coordinates and determines its position in space, e.g., in cartesian coordinates $\mathbf{x}_s = (x, y, h(x,y))$. The surface chemical potential, which acts as the thermodynamic force, is related to the free energy via

$$\mu = \frac{\delta \mathcal{F}}{\delta h} \tag{2.12}$$

and the equation of motion is given by[9]

$$\frac{\partial_t h}{\sqrt{g}} = -\lambda \mu + \eta = -\lambda \sigma \kappa + \eta \ , \tag{2.13}$$

where $\kappa = -\nabla \cdot (\nabla h / \sqrt{g})$ is again the curvature of the surface. Since $\partial_t h/\sqrt{g}$ is the normal velocity of the surface Eq. (2.13) is identical to the Allen-Cahn equation (2.8). We conclude that the dynamical evolution of a nonconserved order parameter (model A) can be completely described by the motion of the domain boundary driven by surface tension. The form of the bulk potential V does not play a role; it determines only the domain wall profile, which has no influence on the growth law (2.8).

2.2 Conserved order parameter

One of the main differences in the theories for a conserved and a nonconserved order parameter is that the dynamics of a conserved order parameter (model B in the classification of Hohenberg and Halperin[4]) cannot be easily described by the motion of the interface alone. Nonetheless, to start, let us first consider purely the case of interface motion, which in this case (because of the conservation law) is described by surface diffusion. Consequently, the normal velocity of the surface obeys a conservation law,

$$v = -\nabla \cdot \mathbf{j} + \nabla \cdot \boldsymbol{\eta}_c \ . \tag{2.14}$$

The surface current $\mathbf{j}$ is driven by the gradient of the surface chemical potential (2.12),

$$\mathbf{j} = -\lambda_c \nabla \frac{\delta \mathcal{F}}{\delta h} \ , \tag{2.15}$$

and the noise $\boldsymbol{\eta}_c$, which represents the thermal fluctuations of the surface current, obeys the fluctuation-dissipation theorem

$$\langle \boldsymbol{\eta}_c(\mathbf{x}_s, t) \rangle = 0 \quad \text{and} \quad \langle \eta_{c,i}(\mathbf{x}_s, t) \eta_{c,j}(\mathbf{x}_s', t') \rangle = 2 k_B T \lambda_c \delta_{ij} \delta(\mathbf{x}_s - \mathbf{x}_s') \delta(t - t') \ .$$

Therefore, the equation of motion for the surface differs from (2.8) by an extra Laplace operator* on the right hand side, and the conserved noise $\boldsymbol{\eta}_c$,

*In principle, the differential operators in Eqs. (2.14)-(2.16) have to be calculated in a local coordinate system attached to the surface[10,11]. In lowest order of h these operators coincide with the usual form in, e.g., cartesian coordinates.

$$v = \lambda_c \sigma \nabla^2 \kappa + \nabla \cdot \boldsymbol{\eta}_c \ . \tag{2.16}$$

Thus, neglecting the effects of the noise, the same dimensional analysis for the average radius of a growing domain, which led to $z = 2$ for the nonconserved order parameter, now yields

$$z = 4 \tag{2.17}$$

for surface diffusion.

After this discussion of surface diffusion we turn to the problem of domain growth for a conserved order parameter (model B). Again, we have a continuity equation, in this case for the magnetization

$$\partial_t \Phi = -\nabla \cdot \mathbf{j} + \nabla \cdot \boldsymbol{\eta} \tag{2.18}$$

and the current $\mathbf{j}$ is proportional to the gradient of the chemical potenial, which is obtained as the functional derivative of the free energy functional (2.1). Thus, the Langevin equation for the conserved Ising-like order parameter reads

$$\partial_t \Phi = \lambda \nabla^2 \left[-c \nabla^2 \Phi + V'(\Phi) \right] + \nabla \cdot \boldsymbol{\eta} \ . \tag{2.19}$$

Eq. (2.19) is sometimes called the Cahn-Hilliard equation[12,13]. Equilibrium properties like the surface tension (2.3) are the same as for the nonconserved order parameter. The Cahn-Hilliard equation (2.19) has the form of a nonlinear diffusion equation. But in contrast to the case of pure surface diffusion, where spins were only allowed to diffuse along the surface, the conservation law for the bulk order parameter now allows single spins to diffuse through domains of the antiphase. This leads to a nonlocal coupling of the domain boundaries and will turn out to be the dominant growth process in the conserved case.

In the following the noise $\boldsymbol{\eta}$ will be set to zero. This will be justified in the next section. Let us first look at a spherical droplet of down-spins immersed in a sea of up-spins. The center of the droplet shall be at $r = 0$ and its radius is R. Such a droplet is stationary only if there is a nonzero constant chemical potential μ: Then Eq. (2.12) reads[†]

$$-c \left[\frac{d^2\Phi}{dr^2} + \frac{d-1}{r} \frac{d\Phi}{dr} \right] + V'(\Phi) = \mu \ . \tag{2.20}$$

In the limit $r \to \infty$ we have $\mu = V'(\Phi(\infty))$. Therefore, a nonzero chemical potential μ requires that $\Phi(\infty) \equiv \Phi_{\rm sd}$ differs from the equilibrium value Φ_0 for a stationary droplet. Thus, if μ is small, the order parameter approaches

$$\Phi_{\rm sd} = \Phi_0 - \mu / V''(\Phi_0) \tag{2.21}$$

for $r > R$. Multiplying Eq. (2.20) by $d\Phi/dr$ and integrating over the radial coordinate r we obtain that

$$\mu \left[\Phi_{\rm sd} - \Phi(0) \right] - V(\Phi_{\rm sd}) + V(\Phi(0)) = -c \int_0^\infty dr \, \frac{d-1}{r} \left(\frac{d\Phi}{dr} \right)^2 \ . \tag{2.22}$$

[†]We restrict ourselves again to the case of a symmetric potential $V(\Phi) = V(-\Phi)$. The more general case does not lead to different results, see Ref. 14.

In the limit $R \to \infty$ the planar interface is obtained and μ goes to zero. Thus, for large radii R we can expand (2.22) in lowest order in $1/R$ and $\Phi_{\rm sd} - \Phi_0$. The result is the usual Gibbs-Thompson relation for liquid droplets[15],

$$\mu = \kappa\sigma/\delta\Phi \quad \text{with} \quad \kappa = (d-1)/R \ , \tag{2.23}$$

where $\delta\Phi \simeq 2\Phi_0$ is the jump of the order parameter at the domain boundary. After the quench, many droplets of different sizes are present. Since a difference in size corresponds to a difference $\delta\mu$ in the chemical potential (2.23) it follows that there will be a diffusion current $\mathbf{j} \sim -\lambda\nabla\delta\mu$, which is directed from the smaller droplets to the larger ones. This is the dominant growth process for a conserved Ising-like order parameter. Consequently, small droplets shrink and large droplets grow. The radial component $j_r(R) \sim R^{-2}$ of this current determines the growth rate of the droplet,

$$\int_{V(R)} d^d x \, \partial_t \Phi = - \int_{S(R)} d^{d-1} x \, j_r(R) \ , \tag{2.24}$$

where $V(R)$ is the volume and $S(R)$ the surface area of the droplet. For a spherical droplet (2.24) reduces to $\delta\Phi\dot{R} = j_r(R)$. Thus we arrive at

$$\frac{dR}{dt} \sim \frac{\lambda(d-1)\sigma}{(\delta\Phi)^2 R^2} \tag{2.25}$$

for a growing droplet. From (2.25) we readily obtain the Lifshitz-Slyozov-Wagner growth law $R(t) \sim t^{1/3}$ for the average domain size, i.e.,

$$z = 3 \tag{2.26}$$

for a conserved scalar order parameter. In the above argument we have assumed that there is only one dominant length scale, the average domain size $R(t)$. Otherwise this kind of dimensional analysis, which goes back to Huse[16], would not be valid. The driving force for the growth of the domains is the difference in the chemical potential (2.23). Thus again, the growth is driven by surface tension and curvature, but the diffusive motion of the spins required by the conservation law leads to a slower growth than in the nonconserved case. On the other hand the growth is faster than pure surface diffusion since the motion of single spins is no longer confined to the surface of the droplet.

In the case of $d = 3$ dimensions the diffusion of spins through domains of the opposite magnetization has been described in more detail[2,3,13,14]. This approach is limited to small concentrations of minus spins, say, in a large sea of plus spins ("off-critical quench") so that the distance between droplets of minus spins is large compared to their radius. Under these circumstances one may incorporate the diffusion process of minus spins through domains of positive magnetization through a simple diffusion equation: Far from the domain boundaries the order parameter is approximately constant. Thus, Eq. (2.19) can be linearized around this bulk value in this regime. Neglecting higher derivatives of the order parameter within the domains [at late times the ratio of $\nabla^4\Phi$ to $\nabla^2\Phi$ scales as $R^{-2}(t)$] one obtains the diffusion equation

$$\partial_t \Phi = \lambda V''(\Phi_0)\nabla^2\Phi \ . \tag{2.27}$$

The change in the order parameter field due to the movement of the domain walls occurs on a time scale $R/\dot{R}$. However, the diffusion field far away from the interfaces relaxes much faster: The relevant time scale is $R^2/[\lambda V''(\Phi_0)]$ for a droplet of radius

R. Therefore, far away from the domain walls the quasi-stationary version of (2.27), $\nabla^2\Phi = 0$, can be used, the solution of which obeys

$$\Phi(r,t) = \Phi_\infty + \frac{b(R)}{r} \ , \tag{2.28}$$

where Φ_∞ is the order parameter far away from the domain wall. If $\Phi_\infty < \Phi_{\rm sd}$ the droplet grows by absorbing spins from the supersaturated majority phase. Consequently the supersaturation $\Phi_0 - \Phi_\infty(t)$ depends on time. The condition $\Phi_\infty < \Phi_{\rm sd}$ is equivalent to the requirement that the droplet radius has to be larger than the critical radius of nucleation

$$R_c(t) = \frac{\sigma}{\Phi_0 V''(\Phi_0)[\Phi_0 - \Phi_\infty(t)]} \ . \tag{2.29}$$

Inside the droplet the solution of the diffusion equation (2.27) is constant, $\Phi \simeq \Phi_0$, since the $1/r$ dependence is ruled out because of the singularity at $r = 0$. The R dependence of the constant b in (2.28) can be determined by matching the order parameter (2.28) with the value (2.21) obtained for $r > R$ for the domain wall profile of a stationary droplet,

$$b(R) = \frac{\sigma}{\Phi_0 V''(\Phi_0)} \left(\frac{R}{R_c} - 1 \right) \ .$$

Using the diffusion current $j_r(R) = -\lambda V''(\Phi_0) \partial\Phi/\partial r|_{r=R} = \lambda V''(\Phi_0) b(R)/R^2$ in (2.24) the equation

$$\frac{dR}{dt} = \frac{D}{R^2} \left(\frac{R}{R_c(t)} - 1 \right) \tag{2.30}$$

for the radius of the droplet is obtained, where all the constants have been absorbed in $D = \lambda\sigma/(2\Phi_0^2)$ and the critical radius of nucleation $R_c(t)$. Droplets with a radius larger than R_c grow, the others disappear. To obtain the $t^{1/3}$ law the time dependence of $R_c(t)$ has to be the same as the time dependence of R itself. This is equivalent to the assumption that there exists only one lengthscale, the average domain size, characterizing the growth of the domains; i.e., in the late stages of growth the size of the droplets and the average distance between the droplets grow in the same way. This result is obtained by studying the continuity equation valid for the droplet size distribution function. One finds that the relation $R_c \sim t^{1/3}$ is indeed fulfilled. Furthermore, the characteristic lengthscale, the average domain size, turns out to be the critical radius $R_c(t)$ itself. For a detailed calculation of $R_c(t)$ the reader is referred to the original papers[2,3].

In $d = 2$ dimensions the approach starting with Eq. (2.27) fails because of the logarithmic solutions of the Laplace equation in two dimensions. Furthermore, the approach is limited to small initial concentrations of the minority phase. However, the dimensional arguments[16], which led to Eq. (2.25), do neither depend on the dimension of the system nor on the concentrations. Several numerical solutions of the Langevin equation (2.19) (see Sec. 6) indeed show that the result (2.25), and therefore (2.26), is correct independently of the dimension of the system and the concentrations. Theoretical approaches that can be applied to these more general situations will be discussed in the following sections. The validity of the result (2.26) has recently also been obtained in a refined theory of Ostwald ripening[17].

The dynamics of a conserved order parameter has been mapped onto the dynamics of a drumhead-type interface model[18], just as in the case of a nonconserved order parameter as described in Sec. 2.1. Now, however, the diffusive modes lead to a nonlocal coupling in the equations for the interface. The eigen-modes of the drumhead model depend on the wavenumber as $\omega \sim q^3$ in agreement with (2.26) and more phenomenological theories[19].

3. RENORMALIZATION GROUP APPROACH

The renormalization group approach to scale-invariant systems, especially critical systems, has proven to be very powerful. But the application of these methods to domain growth problems has been hampered by the absence of a small parameter, e.g., the ϵ expansion for critical systems cannot be applied. Bray's renormalization group (RG) treatment[20,21] of phase ordering is not based on such expansions but exploits the constraints that the conservation law for model B dynamics imposes onto the system. The starting point of Bray's RG theory is the assumption that the growth process can be characterized by a single lengthscale $R(t)$. Therefore, the order parameter correlation function*

$$C(\mathbf{r},t) = \langle \mathbf{\Phi}(\mathbf{r},t)\mathbf{\Phi}(0,t)\rangle \tag{3.1}$$

has the simple scaling form

$$C(\mathbf{r},t) = \Phi_0^2 f(r/R(t)) \ , \tag{3.2}$$

where Φ_0 is again the absolute value of the order parameter at the minimum of the free energy, and the factor Φ_0^2 has been written separately to make the scaling function independent of this value. Consequently, the Fourier transform of $C(\mathbf{r},t)$, the structure factor

$$S(\mathbf{k},t) = \langle \mathbf{\Phi}(\mathbf{k},t)\mathbf{\Phi}(-\mathbf{k},t)\rangle \ , \tag{3.3}$$

has the scaling form

$$S(\mathbf{k},t) = \Phi_0^2 R^d(t) s(kR(t)) \ . \tag{3.4}$$

In (3.1) we allowed for vector order parameters $\mathbf{\Phi}$ with components Φ_α, $\alpha = 1,\ldots,n$. If $n \geq 2$, sharp domain walls and therefore "domains" in the conventional sense do not exist. Nevertheless, for a conserved order parameter the correlation function $C(\mathbf{r},t)$ has oscillatory behavior as in the case of a scalar order parameter. The first zero $r_0(t)$ of $C(\mathbf{r},t)$ may thus be used as a measure of the "domain" size. In fact, for a scalar order parameter r_0 is equivalent to the average radius of the domains. For a nonconserved order parameter one can use, e.g., the length r_0 with $C(r_0,t) = C(0,t)/2$ to define the typical lengthscale. This is what is meant when, in the following, the term 'domain' is used in the context of a vector order parameter.

The starting point for the RG treatment of model B is again the Cahn-Hilliard equation

$$\partial_t \Phi_\alpha(\mathbf{r},t) = \lambda \nabla^2 \frac{\delta \mathcal{F}}{\delta \Phi_\alpha(\mathbf{r},t)} + \nabla \cdot \boldsymbol{\eta}_\alpha(\mathbf{r},t) \ , \tag{3.5}$$

where the conserved noise satisfies

$$\langle \boldsymbol{\eta}_\alpha(\mathbf{r},t)\rangle = 0 \quad \text{and} \quad \langle \eta_{\alpha,i}(\mathbf{r},t)\eta_{\beta,j}(\mathbf{r}',t')\rangle = 2k_B T\lambda \delta_{\alpha\beta}\delta_{ij}\delta(\mathbf{r}-\mathbf{r}')\delta(t-t') \ . \tag{3.6}$$

Eq. (3.5) exhibits the conservation law for the order parameter since the right hand side can be written as the divergence of a current. The free energy functional, now generalized to include vector order parameters, reads

*For simplicity we consider a "critical" quench with $\langle \mathbf{\Phi}\rangle = 0$.

$$\mathcal{F}[\mathbf{\Phi}] = \int d^dx \left[\tfrac{1}{2} \sum_\alpha (\nabla \Phi_\alpha)^2 + V(\mathbf{\Phi}) \right] . \tag{3.7}$$

In the following we will use the form

$$V(\mathbf{\Phi}) = \tfrac{1}{2}\rho \mathbf{\Phi}^2 + \tfrac{1}{4} u \mathbf{\Phi}^4 \tag{3.8}$$

for the potential. For the scalar order parameter ($n = 1$) Eq. (3.8) corresponds to the usual double well potential, whereas for $n = 2$ it has the form of a "Mexican hat". Note, that we will restrict the term "vector order parameter" to this kind of a potential that is invariant under a continuous rotations of the order parameter. As soon as this rotational symmetry is broken and the potential has a finite number of discrete minima we will call the order parameter a "scalar order parameter". The crossover due to such anisotropies has been investigated numerically by Rao and Chakrabarti[22].

Since the RG analysis will be carried out using the momentum-shell method Eq. (3.5) has to be rewritten in terms of the Fourier transforms

$$\mathbf{\Phi}(\mathbf{k}, t) = L^{-d/2} \int d^dr \, \mathbf{\Phi}(\mathbf{r}, t) e^{i\mathbf{kr}} , \tag{3.9}$$

where L^d is the volume of the system. This leads to the transformed Langevin equation

$$\frac{1}{\lambda k^2} \partial_t \Phi_\alpha(\mathbf{k}, t) = -\frac{\delta \mathcal{F}}{\delta \Phi_\alpha(-\mathbf{k}, t)} + \zeta_\alpha(\mathbf{k}, t) , \tag{3.10}$$

which forms basis of the RG calculation. The correlations of the transformed noise ζ obey the fluctuation-dissipation theorem

$$\langle \zeta_\alpha(\mathbf{k}, t) \zeta_\beta(\mathbf{k}', t') \rangle = \frac{2k_BT}{\lambda k^2} \delta_{\alpha\beta} \delta(t - t') \delta_{\mathbf{k}, -\mathbf{k}'} . \tag{3.11}$$

In the momentum-shell method[23] a coarse graining procedure is applied to Eq. (3.10). The reader is encouraged to consult the original article[21] for an excellent description of the underlying philosophy of the approach. The method proceeds in several steps. First, the Fourier modes $\mathbf{\Phi}(\mathbf{k}, t)$ with $\Lambda/b < k < \Lambda$ are eliminated by perturbatively solving the Langevin equation (3.10) for these modes. Here, $\Lambda \sim 1/L$ is the original cutoff of the wavevector $\mathbf{k}$. This first step is usually the most difficult one of the whole procedure[23]. As we will see below, domain growth phenomena are governed by the $T = 0$ fixed point of the RG procedure. In contrast to the critical fixed point, the perturbation expansion cannot be carried out at the $T = 0$ fixed point because of the absence of an expansion parameter. Bray[20,21], however, recognized that such an explicit calculation is not necessary for model B because of the constraints due to the conservation law.

In the second step the momentum vector is rescaled, $\mathbf{k} = \mathbf{k}'/b$, so that $\mathbf{k}'$ is limited by the original cutoff Λ. Since it is presupposed that the correlation function (3.1) obeys the scaling law (3.2) with $R(t) \sim t^{1/z}$ it is necessary that the time is rescaled accordingly, $t = b^z t'$. Furthermore, the order parameter $\mathbf{\Phi}(\mathbf{k}, t) = b^\chi \mathbf{\Phi}'(\mathbf{k}', t')$ has to be rescaled as well[23]. The scaling form (3.4) implies

$$S(\mathbf{k}', t') = b^{-d} S(\mathbf{k}, t) = b^{2\chi - d} \langle \mathbf{\Phi}'(\mathbf{k}', t') \mathbf{\Phi}'(-\mathbf{k}', t') \rangle \equiv b^{2\chi - d} S'(\mathbf{k}', t') .$$

Since the system is required to be scale invariant, i.e., $S'(\mathbf{k}', t') = S(\mathbf{k}', t')$, the exponent χ must be related to the dimension of the system,

$$\chi = d/2 . \tag{3.12}$$

In the RG procedure these two steps are iterated leading to a successive elimination of short wavelengths, which do not to contribute to the scaling behavior. As the iteration proceeds the dynamical coefficient λ, the temperature T, the form of the free energy functional $\mathcal{F}$ and of the correlator (3.11) change until they converge to their fixed point values. At the fixed point also the free energy functional will obey scaling,

$$\mathcal{F}[b^{\chi}\mathbf{\Phi}'(\mathbf{k}',t')] = b^{y}\mathcal{F}[\mathbf{\Phi}'(\mathbf{k}',t')] \ . \tag{3.13}$$

The perturbation expansion mentioned above is usually carried out for the response function

$$G(k,\omega) = \langle \partial\Phi_{\alpha}(\mathbf{k},\omega)/\partial\zeta(\mathbf{k},\omega)\rangle \ , \tag{3.14}$$

where the order parameter field $\mathbf{\Phi}$ and the noise have been fourier transformed in time as well. In the linear theory ($u = 0$)

$$G_0(k,\omega) = \left[-\frac{i\omega}{\lambda k^2} + \rho + k^2\right]^{-1} \tag{3.15}$$

is obtained, whereas for $u \neq 0$

$$G(k,\omega) = \left[-\frac{i\omega}{\lambda k^2} + \rho + k^2 + \Sigma(k,\omega)\right]^{-1} \tag{3.16}$$

where the self-energy Σ must be calculated perturbatively. The crucial point in Bray's theory is the following: From the RG theory for model B for the critical fixed point it is known[4,24] that *there are no terms in the complete perturbation expansion of* $\Sigma(k,\omega)$ *which behave like* $i\omega/k^2$ in the limit when ω and k go to zero, i.e., $\lim_{\omega\to 0}\partial\Sigma(k,\omega)/\partial\omega$ is an analytic function in k. Therefore, the dynamical coefficient λ is not renormalized, but stays at its bare value. For critical systems this leads to the result that for model B the dynamical exponent z is not an independent exponent, but is related to the static exponent η, which describes the decay of the order-parameter correlation function at the critical point[23], through $z = 4 - \eta$. For the $T = 0$ fixed point we will see that this fact can be used to determine the dynamical exponent z as well.

Assuming that the free energy functional $\mathcal{F}$ has attained its fixed point form the two RG steps described above can be applied and the rescaled equation

$$\frac{b^{2-z+\chi}}{\lambda k'^2}\partial_{t'}\Phi'_{\alpha}(\mathbf{k}',t') = -b^{y-\chi}\frac{\delta\mathcal{F}}{\delta\Phi'_{\alpha}(-\mathbf{k}',t')} + \zeta_{\alpha}(\mathbf{k}'/b, t'b^{z}) \tag{3.17}$$

is obtained. Multiplying (3.17) with $b^{\chi-y}$ yields

$$\frac{b^{2-z+2\chi-y}}{\lambda k'^2}\partial_{t'}\Phi'_{\alpha}(\mathbf{k}',t') = -\frac{\delta\mathcal{F}}{\delta\Phi'_{\alpha}(-\mathbf{k}',t')} + \zeta_{\alpha}'(\mathbf{k}',t') \ . \tag{3.18}$$

The correlation function of the rescaled noise ζ' obeys

$$\langle\zeta_{\alpha}'(\mathbf{k}',t')\zeta_{\beta}'(-\mathbf{k}',\tau')\rangle = \frac{2k_BT}{\lambda k'^2}b^{2-z+2\chi-2y}\delta_{\alpha\beta}\delta(t'-\tau') \ . \tag{3.19}$$

Thus, Eq. (3.18) can be cast into the form of (3.10) if the dynamical coefficient is rescaled in the following way

$$1/\lambda' = b^{2-z+2\chi-y}/\lambda \ . \tag{3.20}$$

The requirement that λ remains unchanged determines the dynamical exponent

$$z = 2 + d - y \ . \tag{3.21}$$

The noise correlator (3.19) has the same form as in (3.11) if the temperature is rescaled according to

$$T' = b^{-y} T \ , \tag{3.22}$$

where the result for the dynamical exponent (3.21) has been used. Since $y > 0$ (see below) the temperature (3.22) is reduced under rescaling. This proves that domain growth is indeed governed by the $T = 0$ fixed point, and that the temperature is an "irrelevant variable".

The exponent y determines how the free energy changes under rescaling. Coarse graining leads to configurations with increased order since the ratio of volume to surface area of the domains increases. Therefore, the exponent y is positive at the $T = 0$ fixed point. It can be determined by studying the energy of a spherical domain or, even more simply, by looking at the size dependence of the free energy for a system of size L^d with antiperiodic boundary conditions in one direction and periodic boundary conditions in the others. The stationary solution of Eq. (3.5) with the potential (3.8) yields, for a scalar order parameter ($n = 1$), the domain wall profile

$$\Phi(x) = \Phi_0 \tanh(x/\xi) + \mathcal{O}(e^{-2L/\xi}) \quad \text{with} \quad \Phi_0 = \sqrt{|\rho|/u} \ , \tag{3.23}$$

where $\xi = 1/\sqrt{2|\rho|}$ is the width of the domain wall. The free energy scales like the surface tension (2.3) times the domain wall area and therefore, $y = d - 1$ and $z = 3$ for the scalar order parameter as found in the previous section.

For a vector order parameter the stationary solution of (3.5) for the antiperiodic boundary conditions described above is a continuous twist, e.g., for $n = 2$

$$\begin{aligned} \Phi_1(x) &= \Phi_L \sin(qx) \\ \Phi_2(x) &= \Phi_L \cos(qx) \end{aligned} \qquad \text{with} \quad q = \pi/L \quad \text{and} \quad \Phi_L^2 = \Phi_0^2(1 - q^2/|\rho|) \ . \tag{3.24}$$

The gradient term $(\nabla \mathbf{\Phi})^2 = q^2 \Phi_L^2 \sim L^{-2}$ gives the dominant contribution to the free energy. Terms stemming from the potential, $V(\Phi_L) - V(\Phi_0) \sim L^{-4}$, are of higher order. Consequently, $y = d - 2$ and

$$z = 4 \tag{3.25}$$

for the vector order parameter ($n \geq 2$).

Formula (3.21) is the central result of Bray's RG theory. Its validity is subject to the following conditions:

(i) The order parameter must be conserved.

(ii) The system must order in the conventional sense, i.e., $T < T_c$ and, if $T > 0$, $d \geq 2$ for $n = 1$ and $d \geq 3$ for $n \geq 2$.

(iii) We have assumed that $\lambda(T)$ does not vanish in the limit $T \to 0$. This means that the temperature is not "dangerously irrelevant". See Ref. 21 for a discussion of this point. The numerical simulations of the Cahn-Hilliard equation (2.19) that will be discussed in Sec. 6 indeed show that the assumption is justified.

(iv) The standard scaling assumption is built into the theory. If (3.2) and (3.4) are not obeyed the theory is not valid.

(v) We will see in Sec. 5 that in some cases the scaling laws for vector order parameters are modified by logarithmic corrections[25]. These corrections are not included in the theory.

For the nonconserved order parameter Bray's RG theory does not work, since the dynamical coefficient λ is renormalized and therefore an explicit RG calculation would be necessary. If, however, the result $z = 2$ for the nonconserved order parameter is assumed to be correct, the theory can be used to derive a relation between the renormalized dynamical coefficient and the interface width[21].

4. THEORIES FOR THE CORRELATION FUNCTIONS

The calculation of the scaling functions f and s in (3.2), resp. (3.4), is one of the outstanding problems in the theory of phase ordering. For the nonconserved order parameter there exist the theories of Kawasaki *et al.*[26] and Ohta *et al.*[27], which both contain approximations that lead, e.g., to the unphysical result that the width of the domain walls for the scalar order parameter depends on time[28]. In the case of Ohta *et al.*[27] this has been repaired by Oono and Puri[29], but not in a very systematic way. Nevertheless, these approximations lead to quite satisfactory agreement between theory and simulations[27,29,28]. Recently, the theory of Ohta *et al.*[27] has been generalized for vector order parameters[30].

In the first subsection the limit $n \to \infty$ will be discussed and we will see that the standard scaling assumption is violated in this limit for the conserved order parameter[31]. In Sec. 4.2 the approximate theory due to Mazenko[32,33] is presented. Whereas the theories mentioned above have been applied only to the nonconserved order parameter this theory can also be used for conserved order parameters. Furthermore, it has been generalized for vector order parameters as well[34,35]. Mazenko's approach has been also used to show that standard scaling is recovered for the conserved vector order parameter for any finite dimension n of the order parameter[36].

4.1 Multiscaling: The Limit $n \to \infty$

In this section we will see that the scaling hypothesis (3.2), resp. (3.4), is not always valid. Coniglio and Zannetti[31] showed that Eq. (3.5) can be solved exactly in the limit $n \to \infty$ and that a multiscaling form is obtained. The derivation of Coniglio and Zannetti will be discussed in this section. To get a well defined $n \to \infty$ limit, Eq (3.5) has to be slightly modified to

$$\partial_t \Phi_\alpha = \lambda \nabla^2 \left[-\nabla^2 + \rho + \frac{u}{n} \mathbf{\Phi}^2 \right] \Phi_\alpha \tag{4.1}$$

and the structure factor is redefined to be

$$S(\mathbf{k}, t) = \langle \Phi_\alpha(\mathbf{k}, t) \Phi_\alpha(-\mathbf{k}, t) \rangle \ , \tag{4.2}$$

which is independent of α due to the symmetries of (4.1). The noise has been dropped in (4.1), i.e., it is assumed that temperature is an irrelevant variable. In the $n \to \infty$ limit the term $\mathbf{\Phi}^2(\mathbf{r}, t)/n$ in (4.1) can be replaced by its average

$$I(t) = \int \frac{d^d k}{(2\pi)^d} S(\mathbf{k}, t) \ . \tag{4.3}$$

Therefore, the following *linear* equation of motion for the structure factor is obtained,

$$\partial_t S(\mathbf{k},t) = -2\lambda k^2 \left[k^2 + \rho + uI(t)\right] S(\mathbf{k},t) \ . \tag{4.4}$$

The time dependence of $I(t)$ has to be determined selfconsistently. Eq. (4.4) can be solved exactly with the result

$$S(\mathbf{k},t) = S(\mathbf{k},0) \exp\left\{-2\lambda k^2 \left[k^2 t - Q(t)\right]\right\} \tag{4.5}$$

and

$$Q(t) = \int_0^t d\tau \left[|\rho| - uI(\tau)\right] \ . \tag{4.6}$$

The initial values $S(\mathbf{k},0)$ are determined by the initial conditions and can be chosen to be a constant, $S(\mathbf{k},0) = S_0$, for $0 < k < \Lambda$ and $S(\mathbf{0},0) = 0$, assuming again a critical quench. The solution (4.5) can be rewritten as

$$S(\mathbf{k},t) = S(\mathbf{k},0) \exp\left[R^4(t) k_m^4(t)\right] \exp\left[-R^4(t)\left(k^2 - k_m^2(t)\right)^2\right] \ , \tag{4.7}$$

where

$$k_m(t) = \left[\frac{Q(t)}{2t}\right]^{1/2} \tag{4.8}$$

determines the position of the maximum of $S(\mathbf{k},t)$ and

$$R(t) = [2\lambda t]^{1/4} \tag{4.9}$$

is related to the width of the maximum. Since $\dot{Q}(t) = |\rho| - uI(t)$ we can integrate Eq. (4.7) over $\mathbf{k}$ to obtain a differential equation for $Q(t)$. Provided $R(t) > 1/\Lambda$ the k-integral over $S(\mathbf{k},t)$ converges rapidly for large k and can be extended to $k = \infty$ yielding

$$\dot{Q}(t) = |\rho| - uc(d) R^{-d}(t) D_{-d/2}(z) e^{z^2/4} \ , \tag{4.10}$$

with $z = -Q(t)/\sqrt{\lambda/t}$ and $c(d)$ a constant depending on the dimension of the system. In Eq. (4.10), $D_{-d/2}(z)$ is a parabolic cylinder function[37,38].

We now assume that $Q(t)$ grows faster than $t^{1/2}$ for late times. This assumption has to be checked afterwards for self-consistency. In this case we may use the asymptotic form of the parabolic cylinder function[37]

$$D_{-d/2}(-x) \simeq \frac{\sqrt{2\pi}}{\Gamma(d/2)} x^{d/2-1} e^{x^2/4} \ .$$

If we furthermore assume that $\dot{Q}(t)$ vanishes in the limit $t \to \infty$ we obtain that

$$R^d(t) = \tilde{c}(d) \left[R(t) k_m(t)\right]^{d-2} e^{[R(t)k_m(t)]^4} \ , \tag{4.11}$$

where $\tilde{c}(d)$ is another constant. This equation is solved asymptotically by $k_m(t)R(t) = (\frac{d}{4}\ln t)^{1/4}$. Therefore, the peak position of $S(\mathbf{k},t)$ behaves at late time as

$$k_m(t) \simeq \left(\frac{d}{8\lambda}\frac{\ln t}{t}\right)^{1/4} \ , \tag{4.12}$$

and the assumptions made turn out to be valid. The result (4.11) can be used to rewrite the structure factor as

$$S(\mathbf{k},t) \sim S_0 \left[R^2(t) k_m^{2-d}(t)\right]^{p(k/k_m(t))} \;, \tag{4.13}$$

with

$$p(x) = 1 - (x^2-1)^2 = x^2(2-x^2) \; . \tag{4.14}$$

Eqs. (4.12)-(4.14) are the main results of Coniglio and Zannetti[31]. The structure factor does not obey the standard scaling law (3.4). Rather each k-mode grows with a different exponent,

$$S(\mathbf{k},t) \sim t^{\frac{d}{4}p(k/k_m(t))}$$

apart from logarithmic factors. The function $p(x)$ is shown in Fig. 3. The maximum of S grows with an exponent $d/4$, whereas the other k-modes grow more slowly, in fact modes with $k > \sqrt{2}k_m(t)$ decay. The origin of the multiscaling form (4.13) lies in the

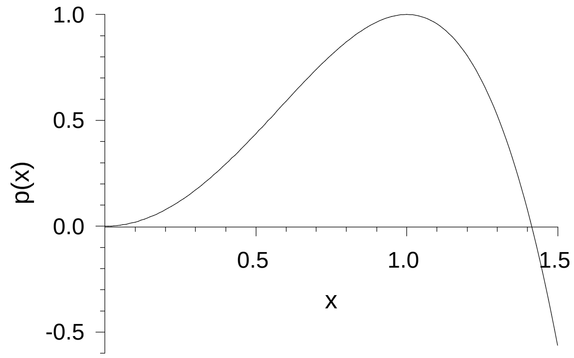

Figure 3. Exponent $p(x)$ of the multiscaling form (4.13).

existence of the two logarithmically different length scales $k_m(t)$ and $R(t)$. Whether the multiscaling behavior found for $n=\infty$ carries over to finite n will be discussed in Secs. 4.2 and 6.

The equations for the nonconserved order parameter (model A) can be solved exactly in the limit $n \to \infty$ as well[31], but in this case the standard scaling assumption is obeyed with $z = 2$ and no multiscaling behavior is found.

4.2 Mazenko's Approach

Mazenko's theory[32,33] provides a new, more systematic, approximate approach to the calculation of scaling functions. Its key element is the division of the order parameter field Φ into two parts:

$$\Phi(\mathbf{r},t) = \Psi(\mathbf{r},t) + \zeta(\mathbf{r},t) \; . \tag{4.15}$$

The first part, Ψ, describes the motion of the interfaces, whereas the second part, ζ, describes fluctuations around that interface profile. A common element of all theories of phase ordering phenomena[26–28,32,33] is the replacement of the (mean) order parameter field Ψ by a field m through a nonlinear transformation $\Psi = \Psi[m(\mathbf{r},t)]$. Mazenko's choice for this transformation is to define m through the equation for a single domain wall (2.2):

$$\frac{d^2\Psi}{dm^2} = V'[\Psi] \tag{4.16}$$

subject to the boundary conditions

$$\Psi(0) = 0 \qquad \text{and} \qquad \lim_{|m|\to\infty} \frac{d\Psi}{dm} = 0 \ . \tag{4.17}$$

Here, the constant c in (2.1) has been scaled to 1. For the potential (3.8) the transformation from Ψ to m is given by Eq. (3.23), $m(\mathbf{r},t) = \xi \operatorname{arctanh}[\Psi(\mathbf{r},t)/\Psi_0]$. Thus, m is equivalent to the coordinate u_1 in Sec. 2 and can be regarded as a field, which determines the position of the interfaces. The generalization of (4.16) for vector order parameters is straightforward and will be discussed further below.

In lowest order the coupling between the fields Ψ and ζ is neglected. For the nonconserved order parameter the equation for the correlation function $C(\mathbf{r},t) \simeq \langle\Psi(\mathbf{r}+\mathbf{x},t)\Psi(\mathbf{x},t)\rangle$ therefore has the form

$$\partial_t C(\mathbf{r},t) = 2\lambda\left[\nabla^2 C(\mathbf{r},t) - \langle\Psi''[m(\mathbf{x},t)]\Psi[m(\mathbf{x}+\mathbf{r},t)]\rangle\right] \ . \tag{4.18}$$

Mazenko then makes the assumption that the field m has a gaussian probability distribution. The same approximation is also incorporated into the theory of Ohta *et al.*[27] The validity of this assumption is not fully understood. Nevertheless, we will see that within this approximation many results of the previous sections will be recovered. However, more complicated correlation functions, which have been obtained with the help of Mazenko's approach[39], show significant deviations from simulation data. This discrepancy has been attributed to the gaussian approximation[39]. The gaussian assumption has been criticized by Yeung *et al.*[40] For the conserved order parameter they find, using the method of Oono and Puri[29], that it leads to a violation of the conservation law, namely $S(\mathbf{k}=0,t) \neq 0$. Furthermore, for small k even negative values of $S(\mathbf{k},t)$ are observed. Recently, a proposal for the systematic improvement of the gaussian approximation has been made[28].

With the help of the gaussian approximation the second term on the right hand side of (4.18) can be expressed in terms of C itself[32],

$$\partial_t C = 2\lambda\left[\nabla^2 C + \frac{\Psi_0^2}{a(t)}\tan\left(\frac{\pi C}{2\Psi_0^2}\right)\right] \tag{4.19}$$

with $a(t) = \pi\langle m^2(\mathbf{r},t)\rangle$. At late times the second moment of the gaussian distribution behaves as[32] $\langle m^2(\mathbf{r},t)\rangle \sim R^2(t)$, which is consistent with the interpretation of $m(\mathbf{r},t)$ as a length. Eq. (4.19) is a closed equation for $C(\mathbf{r},t)$. Furthermore, it has a scaling solution: using the scaling ansatz (3.2) in (4.19) one finds a solution if $R\dot{R} = const$ in agreement with the Allen-Cahn result (2.10). The remaining equation for the scaling function f reads

$$-\mu\mathbf{x}\nabla f(\mathbf{x}) = \tan\left(\frac{\pi}{2}f\right) + \nabla^2 f \tag{4.20}$$

with $\mu = const$. Assuming that the system is isotropic the problem is thus reduced to an ordinary differential equation for the scaling function f. For small arguments $x = r/R$ the solution behaves like $f(x) \simeq 1 - 2\epsilon(x)/\pi$ and $\epsilon(x) \ll 1$. Therefore, the small x behavior can be obtained[32] by expanding (4.20) for small ϵ

$$f(x) \simeq 1 - \left(\frac{2}{\pi(d-1)}\right)^{1/2} x + \cdots \ . \tag{4.21}$$

The result (4.21) is known as Porod's law[41], which is related to the existence of sharp interfaces. We will see below and in Sec. 5, how this law is modified if more complicated defects than domain walls are present. Since x is related to the radial coordinate r the linear behavior of f for small x implies that the scaling function f is nonanalytic for $x \to 0$. Porod's law (4.21) is also reflected in a power law tail, $s(q) \sim q^{-(d+1)}$, for large q of the structure factor (3.4).

To this point we have only discussed the nonconserved scalar order parameter. The method has also been applied to vector order parameters. In this case the field $\mathbf{m}$ is a vector as well and is analogously defined as[34,35]

$$\nabla^2_{\mathbf{m}} \Psi_\alpha[\mathbf{m}] = \frac{\partial V}{\partial \Psi_\alpha} \ , \tag{4.22}$$

where $\mathbf{\Psi}$ with components Ψ_α, $\alpha = 1, \ldots, n$ is the analogue of the field Ψ for the scalar order parameter. One now looks for spherically symmetric solutions of (4.22),

$$\mathbf{\Psi} = \hat{\mathbf{m}} A(|\mathbf{m}|) \ , \tag{4.23}$$

with $\hat{\mathbf{m}} = \mathbf{m}/|\mathbf{m}|$ and boundary conditions $A(0) = 0$ and $A(\infty) = \Psi_0$. The amplitude $A(m)$ therefore obeys the ordinary differential equation

$$A'' + \frac{(n-1)}{m} A' - \frac{(n-1)}{m^2} A = \frac{\partial V}{\partial A} \ . \tag{4.24}$$

Eq. (4.22) together with the boundary conditions specify the order parameter profile around a static defect in equilibrium[34,35]. Topologically stable defects correspond to configurations that cannot be removed by *local* rotations of the order parameter. The only topologically stable defects for $n = 1$ are domain walls, for $n = 2$ they are vortices in $d = 2$ and vortex strings in $d = 3$, and for $n = 3 = d$ they are hedgehogs (see Fig. 4). In analogy to the scalar case we can interpret the field $\mathbf{m}$ as a position vector in the real d-dimensional space if the dimension n of the order parameter is not larger than the spatial dimension d. In fact, topologically stable defects exist only if the condition $n \le d$ is fulfilled. For $n < d$ defects are spatially extended, as in the case of vortex lines, and the field $\mathbf{\Psi}$ varies only within the n dimensional planes orthogonal to those defect lines, whereas it is uniform in the other directions. For $n > d$ no stable local defects exist, and it is questionable whether the ansatz (4.22) together with (4.23) captures the essential structures of the ordering process. Therefore, we will restrict ourselves in the following to the case $n \le d$.

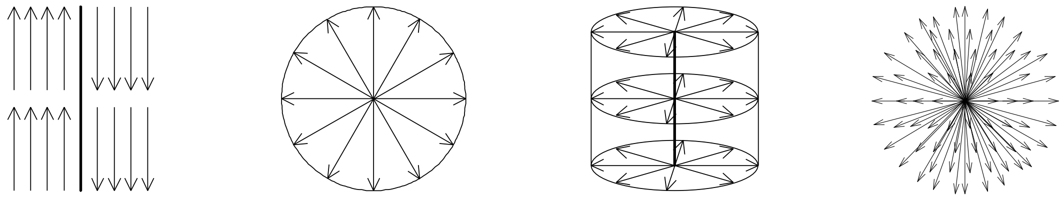

a) b) c) d)

Figure 4. Topologically stable defects: a) domain wall, $n = 1$, b) vortex, $n = 2 = d$, c) vortex line, $n = 2$, $d = 3$, and d) hedgehog, $n = 3 = d$.

The equation of motion for the correlation function reads

$$\partial_t C(\mathbf{r},t) = 2\lambda \left[\nabla^2 C(\mathbf{r},t) - \left\langle \nabla^2_{\mathbf{m}} \Psi[\mathbf{m}(\mathbf{r}+\mathbf{x},t)]\Psi[\mathbf{m}(\mathbf{x},t)]\right\rangle\right] \tag{4.25}$$

in complete analogy to the scalar order parameter. The second term on the right hand side can again be calculated using gaussian averages for the field $\mathbf{m}$ with the result[34,35]

$$\partial_t C = 2\lambda \left[\nabla^2 C + \frac{\gamma}{a}\frac{\partial C}{\partial \gamma}\right] . \tag{4.26}$$

Here, γ and a are related to the moments of the gaussian distribution, $\delta_{ij} g(\mathbf{r}-\mathbf{x},t) = \langle m_i(\mathbf{r},t) m_j(\mathbf{x},t)\rangle$, $a(t) = g(\mathbf{0},t)$, and $\gamma(\mathbf{r},t) = g(\mathbf{r},t)/a(t)$. Note that these moments have to be determined self-consistently from the equation of motion (3.5). The function $C(\mathbf{r},t)$ is given in terms of γ as

$$C(\gamma) = \Psi_0^2 \frac{n\gamma}{2\pi} B^2\left(\frac{1}{2}, \frac{n+1}{2}\right) F\left(\frac{1}{2}, \frac{1}{2}; \frac{n+2}{2}; \gamma^2\right) . \tag{4.27}$$

Here, $B(z,w)$ is the Beta function and $F(a,b;c;z)$ the hypergeometric function[37]. The same result has been obtained[30] using the method of Ohta *et al.*[27] and by studing the motion of defects[42].

In complete analogy with the scalar case one finds that (4.26) has a scaling solution (3.2) with $R(t) \sim t^{1/2}$. Thus, we obtain $z = 2$ regardless of the dimension of the order parameter. However, Porod's law has to be modified. One finds again that the scaling function $f(x)$ is singular in the limit $x \to 0$, and the leading nonanalytic terms behaves as

$$f_{\text{sing}}(x) \sim \begin{cases} x^n & \text{for odd } n \\ x^n \ln x & \text{for even } n \end{cases} . \tag{4.28}$$

This is reflected in a power law tail of the structure factor,

$$s(q) \sim q^{-(d+n)} , \tag{4.29}$$

that is known as the 'modified Porod's law'[30,34,35,42].

The treatment of a conserved order parameter within Mazenko's method contains additional complications, although the equation for the correlation function of the field Ψ can be obtained by applying the operator $-\nabla^2$ onto the right hand side of Eq. (4.19), resp. (4.26). But using the same arguments, which led to $z = 2$ for the nonconserved order parameter, one now finds $z = 4$, which is incorrect for the scalar order parameter as we saw in the previous sections. This is in fact not very surprising, since we learned from the discussion of the nonconserved order parameter that Eqs. (4.19) and (4.26) are obtained by studying the motion of defects, which are domain walls for $n = 1$. But, from the results of Sec. 2 it has become clear that this is not sufficient to describe the dynamics of a conserved scalar order parameter because bulk diffusion becomes the dominant growth mechanism. Therefore, the growth exponent $z = 4$ corresponds to the result (2.17) obtained for pure surface diffusion[43]. To include bulk diffusion in Mazenko's theory the coupling between the fluctuating field ζ, which has been neglected so far, and the order parameter field Ψ must be taken into account[33]. The effect of the fluctuating field ζ on the order parameter field Ψ is the analogue of the diffusion of single spins through the antiphase regime discussed in Sec. 2. The inclusion of ζ leads to a further complication of the theory and will not be discussed here. The reader may consult Ref. 33. The result of the refined theory is the introduction of an additional term in the equation for the correlation function, which then reinstates[33] the Lifshitz-Slyosov-Wagner growth law with $z = 3$. However, as mentioned above, the gaussian assumption for the conserved scalar order parameter can lead to unphysical results[40]. More theoretical work will be needed to clarify this situation.

This leads us to a discussion of the circumstances under which it is legitimate to neglect the effects of the fluctuating field ζ. Quite generally, it must not be neglected if it leads to a faster growth law in comparison to the growth law that is obtained by studying the field Ψ alone. To our present knowledge, the only case for which this is true is the conserved scalar order parameter. We saw that the other results obtained in the previous sections are in agreement with the results obtained here by studying the equations of motion for Ψ.

From the discussion above, it follows that we can use the equation

$$\partial_t C = -2\lambda \nabla^2 \left[\nabla^2 C + \frac{\gamma}{a} \frac{\partial C}{\partial \gamma} \right] . \tag{4.30}$$

for the conserved vector order parameter. The symbols have the same meaning as in Eq. (4.26). This equation has been used by Bray and Humayun[36] to investigate the large n limit of the conserved vector order parameter. As we saw in Sec. 4.1 the standard scaling assumption (3.4) is violated in the limit $n \to \infty$ and it is therefore essential to recognize to what extent this result carries over to finite n. If only terms of order $1/n$ are included, Eq. (4.30) simplifies to[36]

$$\partial_t C = -2\lambda \left[\nabla^4 C - \frac{1}{a(t)} \nabla^2 \left(C + \frac{C^3}{n\Psi_0^2} \right) \right] . \tag{4.31}$$

In the limit $n \to \infty$ the multiscaling result of Coniglio and Zannetti[31] is exactly recovered. However, Bray and Humayun[36] show that the last term on the right hand side* of (4.31) reinstates conventional scaling for any finite n. They furthermore find that the characteristic lengthscale depends on the dimension of the order parameter as $R(t) \sim (t/\ln n)^{1/4}$, thus confirming the result $z = 4$ for all finite n.

It should be noted that the modified Porod's law (4.29) is obtained regardless of whether the order parameter is conserved or not[35]. This result can be derived by studying the typical defects in a system with $n \leq d$. Thus, Porod's law reflects the defect structure of the system and does not depend on the dynamics[35]. For systems without stable localized defects ($n > d$) Porod's law no longer applies, and the scaling function s decays exponentially[44]. The growth law $R(t) \sim t^{1/4}$ nevertheless remains valid.

*Strictly speaking Eqs. (4.30) and (4.31) are valid only for $n \leq d$. Thus, the limit $n \to \infty$ also requires $d \to \infty$. However, it is conceivable that for any finite d the $1/n$ expansion correponding to Eq. (4.31) generates nonlinear corrections in the equation. The contribution $\sim C^3$ is the lowest order term in such an expansion. The coefficient may be different in the general case.

5. MOTION OF DEFECTS

The study of the defect structure for $n \leq d$ provides a powerful tool to obtain information about the structure factor[35,42]. It is illuminating to recall Bray's scaling argument for the tail of the structure factor[39]. For $kR(t) \gg 1$, $S(\mathbf{k},t)$ is sensitive to scales much smaller than the average distance $R(t)$ between defects. Thus, for these k modes the structure factor is essentially the sum of the contributions of independent defects and therefore should scale as the defect density ρ_{def}. For domain walls ($n=1$) the density scales like the wall area per volume, i.e., like $R^{-1}(t)$. For $n=2$ the defect density scales either like the number of vortices per area ($d=2$) or like the length of the vortex strings per volume ($d=3$). In both cases we have $\rho_{\text{def}} \sim R^{-2}(t)$. For $n=3$ the density scales as the number of hedgehogs per volume, i.e., $\rho_{\text{def}} \sim R^{-3}(t)$. Generally the defect density scales as $R^{-n}(t)$ for $n \leq d$. This determines the time-dependence of $S(\mathbf{k},t)$ for large k. The scaling law (3.4),

$$S(\mathbf{k},t) = R^d(t)s(kR(t)) \sim R^{-n}(t)k^{-(d+n)} \quad \text{for } kR(t) \gg 1 \ ,$$

then leads immediately to the modified Porod's law (4.29).

In the remainder of this section we will discuss an approach due to Bray and Rutenberg[25] who derive the growth laws by studying the energy dissipation due to the movement of defects. The starting point is the equation of motion in momentum space

$$\partial_t \mathbf{\Phi}(\mathbf{k},t) = -\lambda k^{\mu} \frac{\delta \mathcal{F}}{\delta \mathbf{\Phi}(-k,t)} \tag{5.1}$$

with $\mu = 0$ in the nonconserved and $\mu = 2$ in the conserved case. The energy dissipation is given by

$$de/dt = \int \frac{d^dk}{(2\pi)^d} \left\langle \partial_t \mathbf{\Phi}(\mathbf{k},t) \frac{\delta \mathcal{F}}{\delta \mathbf{\Phi}(\mathbf{k},t)} \right\rangle = -\frac{1}{\lambda} \int \frac{d^dk}{(2\pi)^d} k^{-\mu} \left\langle \partial_t \mathbf{\Phi}(\mathbf{k},t) \partial_t \mathbf{\Phi}(-\mathbf{k},t) \right\rangle \ , \tag{5.2}$$

where e is the mean free energy density. As we already saw in Sec. 3 the energy density is dominated* by the gradient term of the free energy

$$e \sim \langle (\nabla \mathbf{\Phi})^2 \rangle = \Phi_0^2 \int \frac{d^dk}{(2\pi)^d} k^2 R^d s(kR) \ , \tag{5.3}$$

where the scaling law (3.4) has been used and we set $V(\Phi_0) = 0$ for simplicity. If the integral in Eq. (5.3) converges $e \sim R^{-2}$ is obtained. Otherwise, we impose a cutoff for $kR \gg 1$ at the core size $\xi \sim 1/k_{\text{co}}$ of the defect and use the modified Porod's law (4.29), $S(\mathbf{k},t) \sim R^{-n}k^{-(d+n)}$, to evaluate the integral with the result[42,25]

$$e \sim \begin{cases} R^{-n}\xi^{n-2} & \text{for } n < 2 \\ R^{-2}\ln(R/\xi) & \text{for } n = 2 \\ R^{-2} & \text{for } n > 2 \end{cases} . \tag{5.4}$$

This result indicates that for $n > 2$ the defects are irrelevant, whereas the energy density does depend on the core size for smaller n.

The right hand side of (5.2) can be evaluated in a similar way by using the scaling form for the two-time correlation function, $\langle \mathbf{\Phi}(\mathbf{k},t)\mathbf{\Phi}(-\mathbf{k},t') \rangle = \Phi_0^2 k^{-d} \tilde{s}(kR(t), kR(t'))$. This leads to

*For a scalar order parameter $n = 1$ the gradient and the potential terms scale in fact in the same way, see Eqs. (2.2) and (2.3). Since we will exploit only the scaling behavior of the free energy we can use Eq. (5.3) for all $n \geq 1$.

$$\langle \partial_t \mathbf{\Phi}(\mathbf{k},t)\partial_t \mathbf{\Phi}(-\mathbf{k},t)\rangle = \partial_t\partial_{t'}\langle \mathbf{\Phi}(\mathbf{k},t)\mathbf{\Phi}(-\mathbf{k},t')\rangle|_{t=t'} = (dR/dt)^2 R^{d-2}\bar{s}(kR) \qquad (5.5)$$

and therefore, if the convergence of the integral in Eq. (5.2) is presupposed, to $de/dt \sim (dR/dt)^2 R^{\mu-2}$. In the other cases the integral is again dominated by the contributions on scales with $kR \gg 1$. Thus the size of these structures is small compared to the average distance R between the defects. As we learned at the beginning of this section the structure factor in this regime can be determined by the field of a single defect that we may describe through the equation

$$\partial_t \mathbf{\Phi} = \boldsymbol{\omega} \times \mathbf{\Phi} - (\mathbf{v}\cdot\nabla)\mathbf{\Phi} \ , \qquad (5.6)$$

where $\boldsymbol{\omega}$ describes the rotation of the field around the defect and $\mathbf{v}$ is the velocity of the defect. Dimensional analysis suggests $\boldsymbol{\omega} \sim (dR/dt)/R$ and $\mathbf{v}\cdot\nabla \sim (dR/dt)k$ and consequently the velocity term dominates. The assumption $\mathbf{v} \sim dR/dt$ has been justified by Bray and Rutenberg[25]. Using Porod's law (4.29) we arrive at

$$\langle \partial_t \mathbf{\Phi}(\mathbf{k},t)\partial_t \mathbf{\Phi}(-\mathbf{k},t)\rangle \sim R^{-n}k^{-(d+n-2)}(dR/dt)^2 \qquad \text{for} \quad kR \gg 1 \ . \qquad (5.7)$$

Thus, we see that the integral on the right hand side of Eq. (5.2) converges for $n+\mu > 2$ and is otherwise dominated by the contribution near $k \simeq 1/\xi$. The final result is

$$\int \frac{d^dk}{(2\pi)^d} k^{-\mu}\langle \partial_t \mathbf{\Phi}(\mathbf{k},t)\partial_t \mathbf{\Phi}(-\mathbf{k},t)\rangle \sim \left(\frac{dR}{dt}\right)^2 \times \begin{cases} R^{-n}\xi^{n+\mu-2} & \text{for } n+\mu < 2 \\ R^{-n}\ln(R/\xi) & \text{for } n+\mu = 2 \\ R^{\mu-2} & \text{for } n+\mu > 2 \end{cases} . \qquad (5.8)$$

By comparing the results (5.4) and (5.8) the following growth laws are obtained (subject to the constraint $n \leq d$):

$$\text{for } n = 1: \qquad R(t) \sim \begin{cases} t^{1/2} & \text{if } \mu = 0 \\ t^{1/3} & \text{if } \mu = 2 \end{cases} , \qquad (5.9a)$$

$$\text{for } n = 2: \qquad R(t) \sim \begin{cases} t^{1/2} & \text{if } \mu = 0 \\ (t\ln t)^{1/4} & \text{if } \mu = 2 \end{cases} , \qquad (5.9b)$$

$$\text{for } n > 2: \qquad R(t) \sim \quad t^{1/(2+\mu)} \ . \qquad (5.9c)$$

Again, these results do not include cases where the system does not order in the conventional sense, e.g., the two-dimensional XY-model is excluded. In the latter case numerical simulations for the conserved order parameter[45] are consistent with $R(t) \sim t^{1/4}$ although different moments of the structure factor behave slightly different. This may be taken as an indication for scaling violations.

The above calculation again shows that $z = 2$ for a nonconserved order parameter in all cases. The behavior of the conserved order parameter is more complicated: For $n = 1$ the Lishitz-Slyozov-Wagner result is recovered, and for $n > 2$ the result $z = 4$ is obtained in agreement with the RG result of Sec. 3 and Mazenko's theory in Sec. 4.2. But for $n = 2$, the XY-model, the theory predicts an additional logarithmic factor in contrast with previous theories. It is interesting that this logarthmic factor leads to an effective exponent $z_{\rm eff} < 4$, whereas the theory of Coniglio and Zannetti[31] (see Sec. 4.1), valid in the limit $n \to \infty$, predicts a logarithmic correction leading to $z_{\rm eff} > 4$. The logarithmic corrections for the XY-model will be further discussed in the next section.

The above theory can be used to extract corrections to the leading behavior as well[25]. Furthermore, it is independent of the initial conditions, e.g., critical or off-critical quench, and can also be extended to more complicated order parameters than n-component vectors since only the type of the defects and the corresponding form of the power law tail of $S(\mathbf{k},t)$ has to be known.

6. NUMERICAL SIMULATIONS

Numerical simulations are an indispensable method for checking the validity of the theories discussed in the previous sections. This section is restricted to the discussion of numerical integrations of Langevin equations of type (2.4) and (3.5) that provide a direct test of the theories. Monte-Carlo simulations of Ising, XY, Heisenberg or other models can be used, as well, to study ordering phenomena. However, the interpretation of such simulations can be rendered more difficult through additional although irrelevant contributions in the corresponding free energy functional, which may lead to additional corrections to scaling. Furthermore, those simulations usually have to be carried out at finite temperatures, so that the assumption that temperature is an irrelevant variable cannot be tested. Nevertheless, Monte-Carlo simulations of the two-dimensional conserved Ising model[46,47] show that this model obeys the Lifshitz-Slyozov-Wagner growth law with $z = 3$. An interesting variant on such simulations are Monte-Carlo RG studies, which also have been used to test the validity of Porod's law[47].

Since there is no disagreement between different theories about the growth law for the nonconserved order parameter, most of the numerical work that has been done within the last few years concentrates on the conserved order parameter. For the nonconserved case, Bray and Humayun[48], using a fixed-length spin model, study the ordering dynamics in $d = 2$ for a vector order parameter with $n = 2, 3, 4, 5$ at $T = 0$. For $n = 4$ and $n = 5$ they find that the standard scaling assumption is fulfilled with $z = 2$. For $n = 2$ and $n = 3$ they find that scaling is violated. Note, however, that these systems are at their lower critical dimension and order exclusively at $T = 0$. It might well be true that at $T = 0$ defects, i.e., vortices ($n = 2$) and 'Polyakov solitons'[49] ($n = 3$), are frozen in and cause the scaling violations. Eq. (2.4), generalized for a vector order parameter, has been integrated numerically for $n = 2$ in two[50] and three[51,52] dimensions for the nonconserved case. In two dimensions, after an initial crossover, the expected exponent $z = 2$ is observed. For the three dimensional system significant deviations from the $t^{1/2}$ law are found, which may be attributed to corrections to scaling[25]. These problems are apparently not present in the three-dimensional Heisenberg model ($n = 3$) that has been found[53] to obey the scaling laws with $z = 2$.

In the remainder of this section we will discuss in greater detail numerical simulations for a conserved order parameter. First, the methods of discretizing a Langevin equation like Eq. (3.5) will be discussed. This is in fact not special to the conserved order parameter and the same methods can be applied in the nonconserved case. As noted by Grant *et al.*[54] the Langevin equation (3.5) together with the potential (3.8) can be rewritten in the dimensionless form

$$\partial_\tau \tilde{\Phi}_\alpha(\mathbf{x},\tau) = -\nabla^2 \left\{ \nabla^2 \tilde{\Phi}_\alpha(\mathbf{x},\tau) + \tilde{\Phi}_\alpha(\mathbf{x},\tau) \left[1 - \tilde{\mathbf{\Phi}}^2(\mathbf{x},\tau) \right] \right\} + \sqrt{\epsilon}\nabla \cdot \tilde{\boldsymbol{\eta}}_\alpha(\mathbf{x},\tau) \tag{6.1a}$$

and

$$\langle \tilde{\eta}_{\alpha,i}(\mathbf{x},\tau) \tilde{\eta}_{\beta,j}(\mathbf{x}',\tau') \rangle = \delta_{\alpha\beta}\delta_{ij}\delta(\mathbf{x}-\mathbf{x}')\delta(\tau-\tau') \ , \tag{6.1b}$$

where

$$\mathbf{x} = \left(\frac{\rho}{c}\right)^{1/2} \mathbf{r} \ , \quad \tau = \left(\frac{\lambda\rho^2}{c}\right) t \ , \quad \tilde{\Phi}_\alpha = \left(\frac{u}{\rho}\right)^{1/2} \Phi_\alpha \ , \quad \text{and} \quad \tilde{\boldsymbol{\eta}}_\alpha = \frac{\boldsymbol{\eta}_\alpha}{2k_B T \lambda^2 \rho} \left(\frac{c}{\rho}\right)^{1+d/2} .$$

The only remaining parameter of the model is the noise strength

$$\epsilon = \frac{2k_B T u}{\rho^2} \left(\frac{\rho}{c}\right)^{d/2} \ . \tag{6.2}$$

For the rest of this section we will rename time, order parameter and noise again to t, $\mathbf{\Phi}$, and $\boldsymbol{\eta}$. This should not cause any confusion. The Euler method for a step size Δt and mesh size Δx is a common way to discretize Langevin equations of type (6.1) on a quadratic, resp. cubic, lattice[55]:

$$\begin{aligned}\Phi_\alpha(\mathbf{x}_i, t+\Delta t) = \Phi_\alpha(\mathbf{x}_i, t) - \nabla^2 \left\{\Delta t \nabla^2 \Phi_\alpha(\mathbf{x}_i, t) + f_\alpha[\mathbf{\Phi}(\mathbf{x}_i, t)]\right\} \\ + \left(\epsilon \Delta t / \Delta x^{2+d}\right)^{1/2} \Delta x \nabla \cdot \boldsymbol{\eta}_\alpha(\mathbf{x}_i, t)\end{aligned} \tag{6.3}$$

with

$$f_\alpha[\mathbf{\Phi}] = \Delta t \Phi_\alpha (1 - \mathbf{\Phi}^2) \ . \tag{6.4}$$

The index i labels the sites of the lattice and the noise is discretized in the following way:

$$\nabla \cdot \boldsymbol{\eta}_\alpha(\mathbf{x}_i, t) = \frac{1}{\Delta x} \sum_{a=1}^{d} \left[\nu_\alpha^{(a)}(\mathbf{x}_{i_a}, t) - \nu_\alpha^{(a)}(\mathbf{x}_i, t)\right] \ ,$$

with

$$\langle \nu_\alpha^{(a)}(\mathbf{x}_i, t) \nu_\beta^{(b)}(\mathbf{x}_j, t') \rangle = \delta_{\alpha\beta} \delta_{ab} \delta_{ij} \delta_{tt'} \ ,$$

where i_a specifies the nearest neighbor site in the positive a-direction. The Laplace operators in (6.3) have to be interpreted in their discretized version as well. Oono and Puri[56] showed that the stability of the method (6.3) can be improved by choosing a version of the Laplace operator,

$$\nabla^2 y(\mathbf{x}_i) = \frac{1}{\Delta x^2} \left\{ \frac{1}{2} \sum_{<j>_i} [y(\mathbf{x}_j) - y(\mathbf{x}_i)] + \frac{1}{4(d-1)} \sum_{\ll j \gg_i} [y(\mathbf{x}_j) - y(\mathbf{x}_i)] \right\} \ , \tag{6.5}$$

which includes beside nearest neighbor sites ($<j>_i$) also next-nearest neighbor sites ($\ll j \gg_i$) of site i. The same authors also proposed a so-called cell-dynamic method, which replaces the function f_α of the Euler method (6.4) by[56,50]

$$f_\alpha(\mathbf{\Phi}) = \Phi_\alpha \left\{ \frac{1}{[e^{-2\Delta t} + \mathbf{\Phi}^2(1 - e^{-2\Delta t})]^{1/2}} - 1 \right\} \tag{6.6a}$$

or

$$f_\alpha(\mathbf{\Phi}) = A \frac{\Phi_\alpha}{|\mathbf{\Phi}|} \tanh |\mathbf{\Phi}| - \Phi_\alpha \ , \quad A \simeq 1 + \Delta t \ . \tag{6.6b}$$

Oono and Puri[56] argue that this method should be more stable, i.e., allow for a larger time step Δt than the usual Euler method (6.4), since the functions $g(x) = x + f(x)$, with f from (6.6), increase monotonically. The corresponding function g of the Euler method (6.4) is in fact similar to the logistic map, $x_{n+1} = x_n + f(x_n) = a x_n (1 - x_n)$, which behaves chaotically under iteration, whereas the functions (6.6) do not have that property.

However, there is a different source for instabilities in the numerical integration of partial differential equations. Let us consider for the moment the scalar case with the function f set to zero,

$$\Phi(\mathbf{x}_i, t+\Delta t) = \Phi(\mathbf{x}_i, t) - \Delta t \nabla^2 \nabla^2 \Phi(\mathbf{x}_i, t) \ , \tag{6.7}$$

and the usual Laplace operator $\nabla^2 \Phi(\mathbf{x}_i) = \sum_{<j>_i} [\Phi(\mathbf{x}_j) - \Phi(\mathbf{x}_i)]$. For this equation the cell-dynamic methods and the Euler method are identical. Nevertheless, the iteration of (6.7) is unstable[57] unless the times step fulfills the condition $\Delta t < 1/\Delta x^4$. This instability is caused by the highest derivatives of the *linear* terms in a discretized partial differential equation, and this is in the author's experience the most common source of instabilities in the numerical integration of such equations. Since these instabilities appear in the Euler and the cell-dynamic methods in the same way, the latter usually do not allow for a larger time step. This at least was found in the numerical integration of the three-dimensional conserved XY model[58]. Rogers *et al.*[55] use a time step of $\Delta t = 0.3$ in their Euler method for the conserved scalar order parameter, which is the same time step that is commonly used in the cell-dynamic methods[56,50,51,45]. In cases were the cell-dynamic methods do not allow for a larger time step the Euler method is numerically more efficient because of the more complicated form of the function f in the cell-dynamic methods. A detailed stability analysis of the Euler method for the conserved order parameter can be found in Ref. 55, whereas the stability of the cell dynamic methods is discussed in Refs. 56 and 45.

There are methods, which allow for larger time steps than the Euler method. These are usually implicit methods, like the Crank-Nicholson method[57]

$$\begin{aligned}\Phi_\alpha(\mathbf{x}_i, t+\Delta t) = \Phi_\alpha(\mathbf{x}_i, t) - \frac{\Delta t}{2}\nabla^2\Big\{&\nabla^2\Phi_\alpha(\mathbf{x}_i,t) + \Phi_\alpha(\mathbf{x}_i,t)\left[1-\mathbf{\Phi}^2(\mathbf{x}_i,t)\right] \\ &+ \nabla^2\Phi_\alpha(\mathbf{x}_i,t+\Delta t) + \Phi_\alpha(\mathbf{x}_i,t+\Delta t)\left[1-\mathbf{\Phi}^2(\mathbf{x}_i,t+\Delta t)\right]\Big\}\end{aligned} \tag{6.8}$$

that require the solution of a set of nonlinear equations at every time step. Nevertheless the Crank-Nicholson method is in most cases far superior to explicit methods since it allows for much larger time steps. For linear partial differential equations this method is in fact unconditionally stable, i.e., no restriction on the time step exists[57]. In many cases this is also true for nonlinear equations of type (6.8). Unfortunately, this method is difficult to use for Langevin equations with noise regardless of whether the randomness stems from the initial conditions or is incorporated explicitly through a noise term in the equation. The introduction of noise allows the solution of the nonlinear equations only if the time step is sufficiently small. This nullifies the advantage of the method.

Over the last years several results of numerical simulations that establish unambigously the correctness of the Lifshitz-Slyozov-Wagner growth law (2.26)[55,59–61] have been reported. A very convenient way to determine the characteristic length scale $R(t)$ is to measure the first zero $r_0(t)$ of the correlation function $C(\mathbf{r},t)$[55]. Fig. 5a shows the time dependence of r_0 for the conserved scalar order parameter in two dimensions. At early times $t \lesssim 1000$ the data are quite well explained by a power law $r_0(t) \sim t^{1/4}$. But a least-square fit to the data between $t = 2000$ and 50000 gives an exponent $1/z = 0.333$, which is significantly different from the 1/4 that was found in early Monte-Carlo studies of the Ising model (as noted above, more recent Monte-Carlo simulations have obtained good agreement with $z = 3$). The same exponent has been observed for finite temperatures[55], i.e., $\epsilon > 0$, in perfect agreement with the assumption that temperature is an irrelevant variable. The scaling laws (3.2), resp. (3.4), are found to be obeyed at sufficiently late times. This is illustrated in Fig. 5b, where the correlation function $C(r,t)$ has been plotted as a function of the scaling argument $r/r_0(t)$. The data collapse fairly well onto a single curve, the scaling function. Only for very large r are deviations visible, and these may be due to the finite size of the system. For small r the linear dependence of $C(r,t)$ corresponding to Porod's law (4.21) can be seen. Note, that for very small $r < \xi$ there have to be deviations from Porod's law, which is valid for sharp interfaces, whereas ξ in Eq. (3.23) is of the order of three lattice constants[55].

The scaling behavior of the XY model has been investigated independently by Mondello and Goldenfeld[45] for $d = 2$ and by Siegert and Rao[58] for $d = 3$. These were

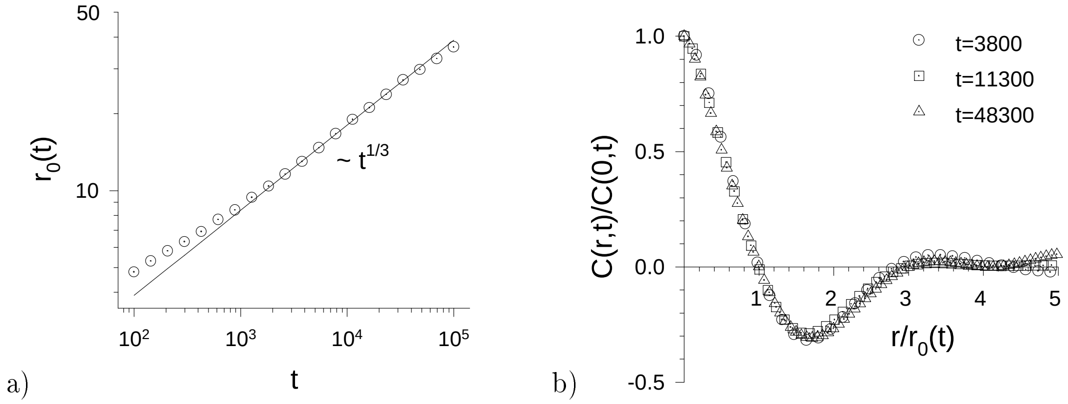

Figure 5. a) First zero of the correlation function $C(r,t)$ obtained by numerical integration of Eq. (6.1) for $n = 1$ in two dimensions. b) Correlation function $C(r,t)$ versus the scaling argument $r/r_0(t)$ for three different times t ($\epsilon = 0$; system size $L^2 = 256 \times 256\Delta x^2$ with $\Delta x = 1.5$).

the first simulations of a system with a conserved vector order parameter, which tried to answer the following questions: Is there an indication for the multiscaling form (4.13), resp. (4.14), and what is the value of the growth exponent z? In $d = 3$ dimensions the influence of finite temperatures was also investigated. Fig. 6 shows the correlation function $C(r,t)$ and the structure factor $S(k,t)$ at two different times. Note, that for $\epsilon > 0$ the limit $C_0(t) = \lim_{r\to 0} C(r,t) \simeq \langle \mathbf{M} \rangle^2$ is different from $C(0,t) \simeq \langle \mathbf{M}^2 \rangle$ marked with an asterix in Fig. 6. Here, $\mathbf{M}$ is the magnetization of the corresponding homogeneous system. It is striking that the data for $C(r,t)$ collapse nicely onto a single curve, but the data for $S(k,t)$ are scattered quite a bit. This is the main reason why the characteristic lengthscale is most easily determined by the first zero $r_0(t)$ of the correlation function $C(r,t)$. The time dependence of $r_0(t)$ for $d = 3$ is shown in Fig. 7. A power law fit to the data results in an exponent $1/z \simeq 0.29$ for $\epsilon = 0$ and $1/z \simeq 0.26$ for $\epsilon = 1$, which both deviate from the growth law $t^{1/4}$ shown as a dotted line in Fig. 7. On the other hand, the multiscaling theory of Coniglio and Zannetti[31] predicts an effective exponent z_{eff} larger than 4 that produces an even worse fit to the data than $t^{1/4}$. The best fit is obtained using the growth law $r_0(t) \sim [t \log(t/\tau)]^{1/4}$ that

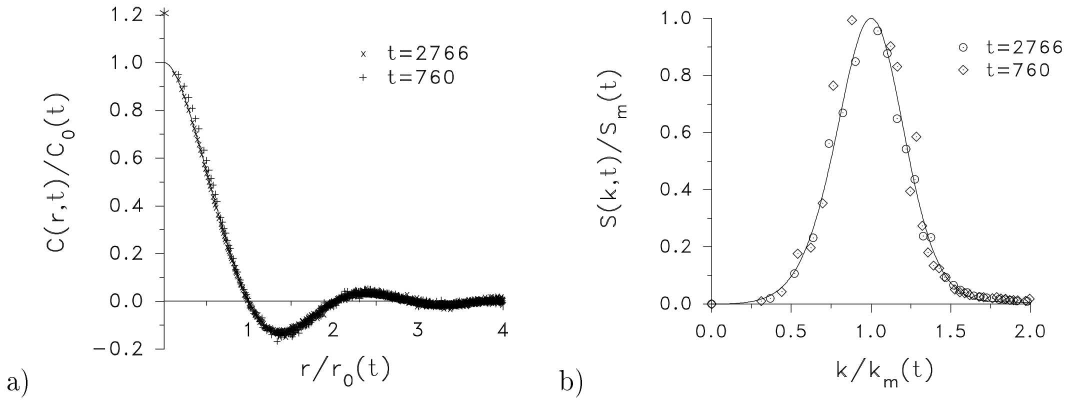

Figure 6. a) Real-space correlation function $C(r,t)$ and b) structure factor $S(k,t)$ for $\epsilon = 1$ and two different times t for $d = 3$. The solid lines correspond to the fit function $C_f(r)$ and its Fourier integral $S_f(k)$ (see text).

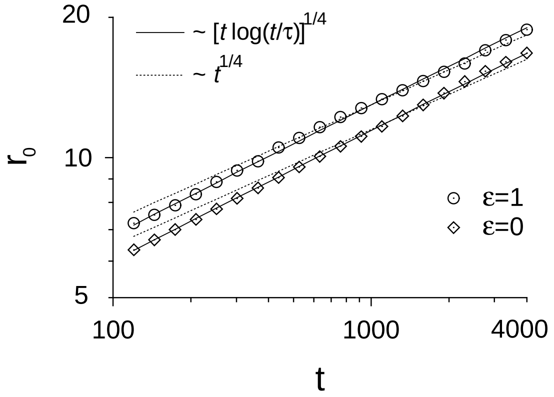

Figure 7. Time dependence of the first zero $r_0(t)$ of the correlation function $C(r,t)$ of the XY model in $d = 3$. The data for $\epsilon = 0$ have been multiplied by a factor of 0.9 to separate them from the data for $\epsilon = 1$.

is predicted by the theory of Bray and Rutenberg[25] (Sec. 5) based on the motion of defects. This fit is also shown in Fig. 7. The result has to be judged with some care: The constant τ is somewhat smaller for $\epsilon = 1$ than for $\epsilon = 0$, but the error bars are fairly large, $\tau \simeq 0.05 - 0.1$. Thus, in principle the result could also be explained by a correction to scaling: The function $(t - t_0)^{1/4}$ fits the data nearly as well. Nevertheless, the agreement with the theory[25] is quite satisfactory. The result suggests that at higher temperatures the mobility of the vortex lines is larger and the deviation from the asymptotic exponent $z = 4$ is therefore smaller.

To distinguish between the standard scaling form (3.4) for $S(\mathbf{k}, t)$ and the multiscaling form (4.13), Coniglio and Zannetti[31] suggested plotting $S(\mathbf{k}, t)$ as a function of t for several fixed values of $x = k/k_m(t)$. On a log-log scale this plot should show several parallel lines with slope $d/4$ if the standard scaling form is applicable, whereas in the case of multiscaling one would see a spread of slopes $p(x)d/4$. However, in a numerical simulation $S(\mathbf{k}, t)$ can be calculated only for a discrete set of k-values because of the finite size of the system and the periodic boundary conditions. Therefore, one has to interpolate somehow between these k-values to obtain the necessary data. Unfortunately, in the late time regime the peak position $k_m(t)$ is already quite small so that the set of k-values in the neighborhood of $k_m(t)$ is not very dense (see Fig. 6b). Additionally as already noted above, fluctuations in $S(\mathbf{k}, t)$ are quite pronounced, even after averaging over 30 independent runs. This makes a linear interpolation between the data points or a least-square fit to some fit function for $S(\mathbf{k}, t)$ very inaccurate. Siegert and Rao have taken a different line of approach. As seen in Fig. 6a, the data for $C(\mathbf{r}, t)$ form a much denser set and are less noisy than the data for $S(\mathbf{k}, t)$. They therefore fitted $C(\mathbf{r}, t)$ to the function $C_f(r) = C_0 j_0(k_0 r) b(r)$ with $k_0 = \pi/r_0$. The modulation of $C(\mathbf{r}, t)$ is extremely well described by $j_0(x) = \sin x/x$, which, remarkably, is consistent with the analytical calculations[36] of Bray and Humayun to $\mathcal{O}(1/n)$. The decay function $b(r)$ was chosen so that the Fourier integral $S_f(k) = \int \frac{d^d k}{(2\pi)^d} C_f(r) \exp(i\mathbf{k}\mathbf{r})$ can be calculated analytically and gives $S_f(0) = 0$ as required by the conservation law. Furthermore, the data indicate that $C(\mathbf{r}, t)$ has a quadratic maximum at $r = 0$ requiring a quadratic maximum for $b(r)$ at $r = 0$ as well. The actual form of the decay function $b(r)$ does not play a large role: several forms have been used without changing the quality of the fit and the results that are derived from it[58]. The function which has been used in Fig. 6 is $b(r) = (1 + ar^2)\exp[-\beta(r^2 + \gamma^2)^{1/2}]$. Here, β and γ are fitting parameters, but a is determined by the condition $S(k=0)=0$.

The Fourier integral $S_f(k)$ was then used as a fit for $S(\mathbf{k},t)$. With this method most of the fluctuations and lattice effects could be eliminated. Both functions $C_f(r)$ and $S_f(k)$ for the time $t=2766$ are shown in Fig. 6 as solid lines. The result of the fit procedure is displayed in Fig. 8. In contrast to the form $p(x)$ (see Fig. 3) predicted by Coniglio and Zannetti[31] the slopes of $S(\mathbf{k},t)$ for fixed values of x show a minimum for $x=1$ (see Fig. 9). This indicates that the asymptotic regime has not quite been reached, and it is quite plausible that the measured form of $p(x)$ will finally approach $p(x)=1$, in agreement with the standard scaling assumption. It should be noted that the accuracy of the fit decreases when $|x-1|$ increases because of the smallness of $S(\mathbf{k},t)$ in the wings. Nevertheless, the data indicate that $S(x,t)$ increases with time for all values of x, whereas the multiscaling form $p(x)=1-(1-x^2)^2$ predicts a decay for $x>\sqrt{2}$, which is inconsistent with the data. The same form of $p(x)$ has been obtained by Mondello and Goldenfeld[45] for the two dimensional XY model. Interestingly, this form is also obtained in a simulation for a conserved scalar order parameter[61]. Since there is no theoretical reason to expect multiscaling in that case this result shows that the form seen in Fig. 9 is in agreement with the standard scaling assumption (3.4).

As already mentioned, and seen in Fig. 6a, the correlation function $C(r,t)$ behaves

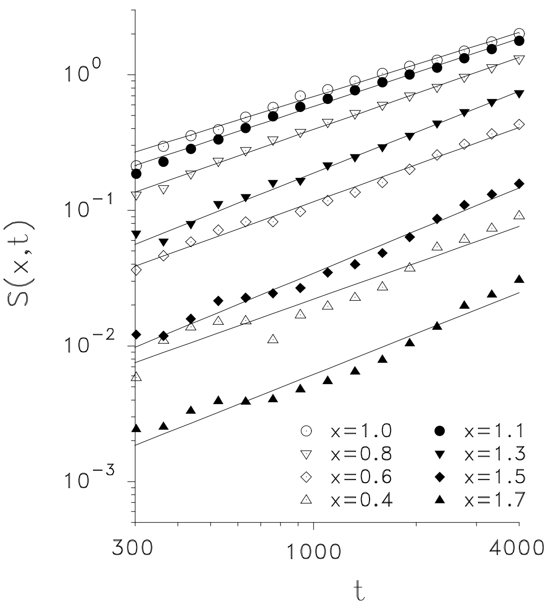

Figure 8. Structure factor $S(x,t)$ for fixed values $x=k/k_m(t)$. The straight lines are power law fits $S(x,t)\sim t^{p(x)d/4}$.

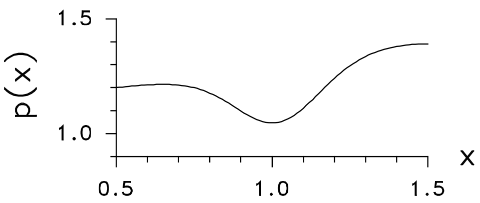

Figure 9. Measured exponents $p(x)$ corresponding to the slopes of the solid lines in Fig. 8.

as $C_0[1-(qr)^2+\ldots]$ for small r. Dimensional analysis then suggests $S(\mathbf{k},t)\sim q^2/k^5$ in agreement with the modified Porod's law (4.29). This is in fact slightly misleading since the power law tail of the structure factor, $S\sim k^{-(d+n)}$ originates from the singular part $f_{\rm sing}(r)\sim r^2\ln r$ for $r/r_0\ll 1$ of the real space correlation function. It is very hard to decide whether the logarthmic factor predicted in Eq. (4.28) can be seen in a numerical result like the one displayed in Fig. 6a. E.g., least-square fits of $C(r,t)$ for small r are not accurate enough to distinguish between a r^2 or $r^2\ln r$ dependence.

7. PATTERN FORMATION IN MOLECULAR BEAM EPITAXY

During the last decade it has become evident that many non-equilibrium growth processes on surfaces display power-law behavior in space and time similar to that found at the critical point of systems undergoing phase transitions. In particular, films grown by deposition processes like molecular beam epitaxy (MBE) reveal a surprising variety of surface morphologies[10]. To model MBE one assumes that overhangs and defects in the growing film can be neglected and that the dominant relaxation process is surface diffusion; thus, desorption from the surface is neglected as well. It follows that the height h describing the local position of the moving surface obeys a conservation law[62,10],

$$\partial_t h(\mathbf{r},t)=-\nabla\cdot\mathbf{j}\left[\nabla h(\mathbf{r},t)\right]+\eta(\mathbf{r},t)\ , \tag{7.1}$$

where η is the shot noise due to the fluctuations of the incoming particle beam, and the height is measured in a comoving frame of reference. The growth process modelled by Eq. (7.1) leads in some cases to scale invariance of the correlation functions. This phenomenon is described within the theories of kinetic roughening. But, in other circumstances, instabilities appear, which mainfest themselves in pyramidal structures on the surface.

In this section we will discuss growth under MBE conditions for systems that have potential barriers near step edges. These barriers suppress the diffusion of adatoms to a lower terrace. This effect was first studied experimentally by Ehrlich *et al.*[63] and was later investigated theoretically by Schwoebel[64]. We will call it the Ehrlich-Schwoebel (ES) effect. The same effect is sometimes called Schwoebel effect or diffusion bias. Its importance for MBE growth has been illustrated by Villain[62], who pointed out that it gives rise to instabilities, which since have been observed in experiments[65–67]. In this section we will see that the temporal evolution of these instabilities is similar, although not identical, to the ordering phenomena described in the previous sections.

The surface current $\mathbf{j}$ is the sum of two parts: Firstly, there is the equilibrium surface diffusion current $\mathbf{j}_{\rm eq}$ (2.15) that has already been discussed in Sec. 2.2. In lowest order in h we have

$$\mathbf{j}_{\rm eq}=D_{\rm eq}\nabla\Delta h\ , \tag{7.2}$$

with a coefficient $D_{\rm eq}$ that is proportional to the surface stiffness[10]. Secondly, there is a nonequilibrium contribution $\mathbf{j}_s=\nabla h f[(\nabla h)^2]$ that is proportional to the incoming flux F. The form of the function f determines the universality class to which the growth process belongs: If $\nu_2=-f(0)>0$ all nonlinearlities and higher order derivatives of h in the equation of motion (7.1) are irrelevant, i.e., they have no influence on the growth law at sufficiently late times. Consequently, the class with $f(0)<0$ is described by the Edwards-Wilkinson equation[68]

$$\partial_t h = \nu_2 \Delta h + \eta \ . \tag{7.3}$$

In the other case $f(0) > 0$ the equation of motion is linearly unstable and the higher order terms become important. We will see below that the growth dynamics under MBE conditions for surfaces with ES barriers are characterized by such a surface current. The Edwards-Wilkinson class and the linearly unstable case are the two generic universality classes for MBE growth[10]. Only in the untypical case $f(0) = 0$ different growth laws may be observed.

In this paragraph we rederive[62,67,69] the form of the contribution $\mathbf{j}_s$ to the surface current due to the ES effect. We assume for the moment that no adatom on a vicinal surface can overcome the barrier at downward steps and therefore all adatoms remain on the terrace on which they have been deposited. If the terrace size l is smaller than the diffusion length l_d basically all adatoms reach the step edge of the upper terrace, where they become incorporated into the substrate. This results in an uphill current $j_s(m) \sim 1/m$, where $j_s = |\mathbf{j}_s|$ and $m = 1/l$ is the tilt of the vicinal surface. All lengths are measured in units of the lattice constant. This is the so-called step-flow regime. If the terrace size is larger than l_d only the adatoms within a distance l_d from the upper terrace will reach that step, creating a depletion zone in its neighborhood. Only this fraction of all adatoms contributes to the current j_s. All other adatoms form islands on the terrace and the corresponding currents average to zero. Thus, the current $j_s(m) \sim l_d/l = l_d m$ has a positive derivative $j_s'(m)$ for small m and this leads to the instability discussed by Villain[62]. The crossover between the two regimes occurs when l is of the order of l_d. The diffusion length depends on the incoming flux F and the diffusion constant D of the adatoms, $l_d \sim (D/F)^\chi$, where the exponent χ depends on the growth conditions[70] and varies between 1/2 and 1/6.

Although $j_s'(m)$ is negative the step-flow regime $j_s \sim 1/m$ is in fact not a regime of stable surface growth[71]. To see this we expand the surface current $\mathbf{j}_s(\nabla h)$ around an average tilt $\mathbf{m}$ with $|\mathbf{m}| = m > 1/l_d$. We introduce the deviations $\nabla \tilde{h}$ from this average tilt through the definition $\nabla h = (m + \partial_\parallel \tilde{h}, \partial_\perp \tilde{h})$ with $|\partial_\parallel \tilde{h}|$, $|\partial_\perp \tilde{h}| \ll m$. Expanding in lowest order of $\nabla \tilde{h}$ we obtain $|\nabla h| \simeq m + \partial_\parallel \tilde{h}$ and therefore

$$\nabla \cdot \mathbf{j}_s \simeq j_s'(m)\, \partial_\parallel^2 \tilde{h} + \frac{j_s(m)}{m}\, \partial_\perp^2 \tilde{h} \ . \tag{7.4}$$

The first term on the right-hand side of (7.4) stabilizes the growth since $j_s'(m) < 0$ in the step-flow regime. But the second term leads to instabilities since $j_s(m)/m$ is always larger than zero. As soon as surface fluctuations lead to a local curvature $\partial_\perp^2 \tilde{h}$ in the direction perpendicular to the tilt that is larger than the curvature $\partial_\parallel^2 \tilde{h}$ along the tilt direction these fluctuations will start to grow [assuming that $|j_s'(m)|$ is of the same order of magnitude as $j_s(m)/m$]. This leads to a fingering instability quite similar to the Mullins-Sekerka instability of planar fronts[72]. Thus, the surface currents caused by ES barriers do not lead to a stable evolution, at least not for two-dimensional surfaces. Therefore, additional effects have to be taken into account, which lead to a consistent description of the growth phenomena. These stabilizing effects will be discussed below.

Recently, Johnson *et al.*[67] proposed a simple analytic form for the current that interpolates between the two regimes,

$$\mathbf{j}_s(\mathbf{m}) \sim \mathbf{m} / \left[1 + (l_d \mathbf{m})^2\right] \ . \tag{7.5}$$

In fact, Krug, Plischke, and Siegert[74] showed for various models that the surface current has this form if ES barriers are present, and the corresponding instabilities have been seen in Monte-Carlo simulations of MBE growth[73,10]. Nevertheless, this equation has to be modified if the growth reaches a regime where the condition $m \ll 1$ is no longer fulfilled, as can be the case in the unstable three-dimensional growth of real materials. Eq. (7.5) was derived for vicinal surfaces, and there is no reason why it should be valid for inclinations m of order 1. We will see below that the current j_s necessarily drives the surface into a regime with $m \gg 1$. To derive a more general form it is useful to express the current (7.5) in terms of the angle of inclination ϑ of the surface with respect to the unstable singular surface: $j_s(\vartheta) = |\mathbf{j}_s(\vartheta)| \sim \tan\vartheta/[1+(l_d \tan\vartheta)^2]$. Thus, $j_s(\vartheta)$ is periodic with a period of π. Therefore, the growing crystal has only one high symmetry surface corresponding to $\vartheta = 0$. However, the form of the current (7.5) is easily generalized to obtain a model for a more realistic crystal symmetry. If we wish to model, e.g., a growing film with cubic symmetry we may use

$$j_s(m) \sim \tfrac{1}{2}\tan(2\vartheta)/\left[1+(\tfrac{1}{2}l_d \tan(2\vartheta))^2\right]$$

or

$$\mathbf{j}_s(\mathbf{m}) = D_s \mathbf{m}(1-m^2)/\left[(1-m^2)^2+(l_d m)^2\right] \ . \tag{7.6}$$

In the step-flow regime[62,67] the current $|\mathbf{j}_s| \simeq F/m$, thus, $D_s = F l_d^2$. The current (7.6) is properly equal to zero on the two equivalent high-symmetry surfaces $\vartheta = 0, \pi/2$ and, moreover, is also equal to zero at the intermediate inclination $\vartheta = \pi/4$ or $m = m_0 = 1$. The generalization for other lattices is straightforward. We note that the form (7.6) still has the correct physical behavior: $j_s \sim m$ for $m \ll 1/l_d$ and $j_s \sim 1/m$ for $1/l_d \ll m \ll 1$. Despite these similarities (7.6) gives rise to a completely different behavior than the current (7.5) as will be shown below.

Certainly, Eq. (7.6) is not exact*. It merely gives an interpolation formula that takes into account the occurence of a zero in j_s and the requirements of the ES effect. The existence of at least one zero ϑ_0 between 0 and $\pi/2$ in the surface current j_s with $j'(\vartheta_0) < 0$ is guaranteed by the continuity of the surface current as a function of the tilt angle ϑ: High symmetry surfaces like the $\{110\}$ surfaces in a cubic crystal cannot be consistently described as vicinal to other surfaces. Rather the symmetries require that the current j_s is zero for such orientations. If $j'(\vartheta_0) < 0$ the homogeneous solution $m(\mathbf{r}) = m_0 = \tan\vartheta_0$ is a stable solution of the corresponding Langevin equation. In that case m_0 turns out to be the selected slope of the evolving surface configuration (see below). If $j'(\vartheta_0) > 0$ there has to be another zero, $j(\tilde{\vartheta}_0) = 0$, with $0 < \tilde{\vartheta}_0 < \vartheta_0$ and $j'(\tilde{\vartheta}_0) < 0$. Note the generality of the argument: We do not even have to know that there is a regime with $j_s \sim 1/m$. We only need Villain's result[62] that $j'(0) > 0$ for high symmetry surfaces with a ES effect.

The appearence of a zero in the surface current j_s for $m \simeq 1$ is quite plausible also from a different point of view: Assuming that the barriers at the step edges have a finite width of roughly one lattice constant[76] these barriers start to overlap as soon as the tilt m is of order 1. Thus, for these slopes the barriers disappear and the current j_s must have a zero around $m \simeq 1$.

From this discussion it is already clear that $m_0 = 1$ is not necessarily the only zero of the current $\mathbf{j}_s$. There are many processes, e.g., knock-out effects[77], which lead to downhill currents that can overcompensate the ES current for large enough slopes. This

*In principle the right hand side of Eq. (7.6) has to be multiplied by a factor $\cos\vartheta$: The current $\mathbf{j}_s$ is proportional to the adatom density[62], which in turn is proportional to the flux $\tilde{F} = F\cos\vartheta$ that reaches the sloped surface. In fact, the incoming particle beam breaks the symmetry, which is implemented in Eq. (7.6) and one can think of additional factors, that do not have the same periodicity. However, we only require $j_s(\vartheta)$ to have a zero for some finite slope. Since the symmetry breaking factors do not add any new qualitative features to the equation they have been neglected in (7.6).

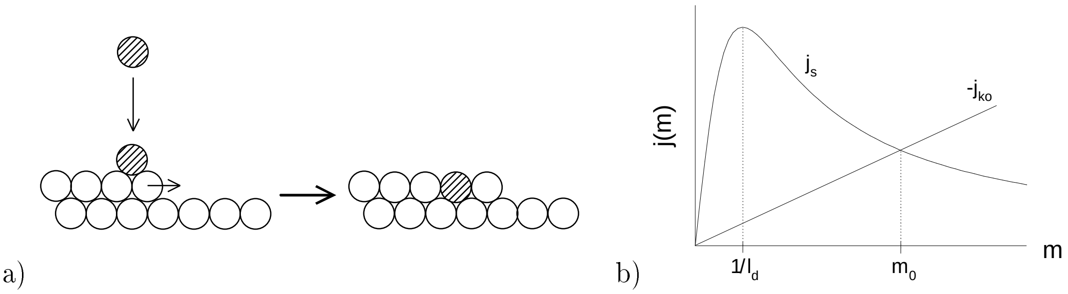

Figure 10. Illustration of the knock-out effect: a) schematic picture of the effect; b) surface currents due to ES effect and knock-out effects compensating each other at $m = m_0$. It is assumed that the diffusion length l_d is so large that the zero in the total current due to the crystal symmetry lies at much larger slopes.

is illustrated in Fig. 10. A freshly deposited particle at the edge of a terrace replaces the edge atom by pushing it along the lower terrace. Since this is indistiguishable from the deposition of a particle, coupled with the movement of that particle to the lower terrace, this corresponds to a downhill current j_{ko}, which is proportional to the number of edge atoms, i.e., to the inclination m of the substrate: $j_{\mathrm{ko}} \sim -m$. Since the diffusion length l_d is usually of the order of 10-100 lattice constants such a zero can appear at fairly small slopes, which may explain the structures observed in the growth of GaAs on GaAs(001) substrates[67,78].

As we just saw there can be other zeros between $m = 0$ and $m = 1$. The selected slope is given by the smallest zero of $j_s(m)$ with $m_0 > 0$. From this point of view Eq. (7.6) is a minimal model: $j_s(m)$ must have at least one zero between 0 and ∞. The exact form of $j_s(m)$ does not play a role. The slope selection mechanism and the growth exponents to be described below do not depend on such details. This is completely equivalent to the ordering phenomena discussed in the previous sections: The exact form of the potential V and the position of its minima Φ_0 do not affect the growth law.

The total surface current $\mathbf{j}$ is the sum of $\mathbf{j}_s$ and the equilibrium surface current $\mathbf{j}_{\mathrm{eq}}$. Eq. (7.1) is readily transformed into an equation for the tilt,

$$\partial_t \mathbf{m} = -\nabla\nabla \cdot \mathbf{j}_s(\mathbf{m}) - D_{\mathrm{eq}}\Delta\Delta\mathbf{m} + \nabla\eta \ , \tag{7.7}$$

where we have used the fact that $\nabla \times \mathbf{m} = 0$. For *one-dimensional* surfaces, Eq. (7.7) is equivalent to the equation of motion of a conserved scalar order parameter as in spinodal decomposition as was already noted by Krug, Plischke, and Siegert[74]. Consequently, "domains" with $m = +m_0$ and $m = -m_0$ are formed and the size of the domains grows with time as $t^{1/3}$, the well-known Lifshitz-Slyozov law[†]. It is illuminating to notice the difference in the dynamical behavior resulting from the current (7.5): In that case the "potential" $V(\mathbf{m}) = -\int dm\, j_s(m) \sim -\ln[1 + (l_d m)^2]$ has minima only at $m_0 = \pm\infty$. Therefore, the slope of the emerging profile never saturates and deep groves develop. Thus, the condition $m \ll 1$ cannot be satisfied for the current (7.5), and this form can only be used for early times[67,78]. The development of deep grooves was also derived by Elkinani and Villain[79] for a similar model.

[†]In the case of a conserved scalar order parameter in one dimension, the growth law at $T = 0$ is logarithmically slow: $R(t) \sim \log t$. For $T > 0$ the $t^{1/3}$ law is recovered[75]. Since the shot noise due to the fluctuating particle beam is always present in growth dynamics of surfaces the case discussed here corresponds to $T > 0$.

Unfortunately most models used for Monte-Carlo simulations correspond to the current (7.5). The solid-on-solid condition employed in these simulation destroys the original symmetries of the growing film and no slope selection occurs[73]. In these cases the growth dynamics seem to be characterized by *two* exponents: For one-dimensional surfaces Siegert and Plischke[10] found that the amplitude $G(0,t)$ of the height-height correlation function $G(r,t) = \langle h(r,t)h(r,0)\rangle$ grows as $t^{1.2}$, whereas the first zero of $G(r,t)$ increases only as $t^{0.17}$.

We now turn to the two-dimensional case. The equilibrium term $D_{\rm eq}\Delta\Delta\mathbf{m}$ in (7.7) has the usual form for ordering dynamics of a vector order parameter $\mathbf{m}$. However, the same is not true for the first term on the right hand side of (7.7), even if $\mathbf{j}_s = \delta\mathcal{F}/\delta\mathbf{m}$ and, of course, there is no guarantee that this current will be derivable from a free energy. Nevertheless, we will see that the dynamical evolution of the surface shows many similarities with the ordering dynamics of a conserved order parameter. The stable solutions for the order parameter in the domain growth problem correspond to the stable surface orientations of the growing structures which are determined by the underlying crystal structure in the present case.

The RG theory discussed in Sec. 3 relates the dynamical exponent $z = 2 + d - y$ to the exponent y that describes how the energy of an elementary excitation scales with the size of the system. To determine the exponent y one only has to know the steady-state solution of the equation of motion. In the present case of surface growth the corresponding equation reads

$$D_{\rm eq}\nabla^2\mathbf{m} + \mathbf{j}_s(\mathbf{m}) = 0 \tag{7.8}$$

with $\mathbf{j}(\mathbf{m})$ given by (7.6). Eq. (7.8) has a solution of type (3.24) and therefore we would expect that the growth process is equivalent to the ordering dynamics of a two-dimensional XY model. But there is an important difference between the slope $\mathbf{m}$ and the order parameter of an XY model: The slope must obey the constraint $\nabla \times \mathbf{m} = 0$, which could make it effectively a one-dimensional order parameter, although Eq. (7.8) shows that for the current (7.6) there are no sharp domain walls in the system. Note the difference in the two equations of motion: For the XY model we have a term $(\nabla\cdot\nabla)\delta\mathcal{F}/\delta\mathbf{m}$ on the right hand side of the equation, whereas for the surface model the corresponding term reads $\nabla(\nabla\cdot\delta\mathcal{F}/\delta\mathbf{m})$. Thus, the two differential operators, grad and div, are exchanged in the two cases!

Eq. (7.1) has been integrated numerically[80] for the current (7.6) with $\eta = 0$ and $\eta > 0$. To classify the growth law the first zero r_0 of the order-parameter correlation function $C(\mathbf{r},t) = L^{-d}\sum_{\mathbf{x}}\langle\mathbf{m}(\mathbf{r}+\mathbf{x},t)\mathbf{m}(\mathbf{x},t)\rangle$ was determined. Fig. 11 shows an almost perfect power law $r_0(t) \sim t^{1/z}$ with $z = 4$. This result suggests that indeed the surface evolution is equivalent to the dynamics of a conserved vector order parameter with $z = 4$. On the other hand the theory of defect dynamics (Sec. 5) is not applicable to the two-dimensional XY-model because of long range correlations between vortices[25]. In fact, numerical simulations[45] show deviations from the $t^{1/4}$ behavior that are not seen in Fig. 11. Whether this can be attributed to the effects of the constraint $\nabla \times \mathbf{m} = 0$ is unclear.

The current (7.6) is a simplification in the sense that it neglects in-plane anisotropies: For cubic symmetry $\mathbf{j}_s$ has to be periodic with a period of $\pi/2$ only for rotations around the [100] and [010] axes, whereas (7.6) has this symmetry for all axes lying in the xy-plane. Thus the above results are valid only on time scales for which such anisotropies in the diffusion current can be neglected. In the more general case we consider a current with components $j_{s,x} = m_x f(m_x^2)$ and $j_{s,y} = m_y f(m_y^2)$ with the same function f defined above. The corresponding "potential" is simply

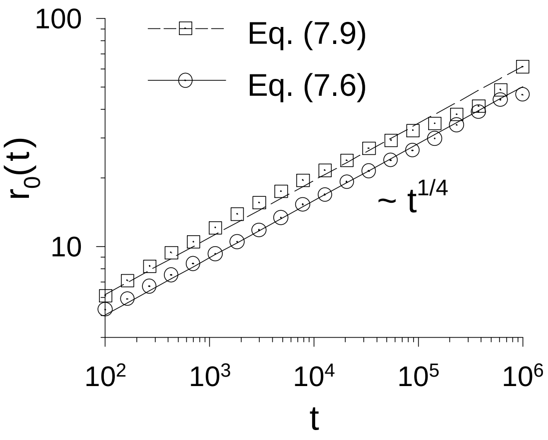

Figure 11. Time dependence of the first zero $r_0(t)$ of the slope-slope correlation function. The lines are power law fits with an exponent $1/z = 0.25$. The system size is $L^2 = 128 \times 128 \Delta x^2$ with $\Delta x = 2$. The parameters $l_d = 10$, $D_{\text{eq}} = 1$, $D_s = 2$ have been used in both cases. The noise η was set to zero.

$V(\mathbf{m}) = -\int dm_x\, j_{s,x} - \int dm_y\, j_{s,y}$. Thus, it has minima at $\mathbf{m} = (\pm 1, \pm 1)$ instead of $\mathbf{m} = (\pm 1, 0)$ and $\mathbf{m} = (0, \pm 1)$ as required. This is easily repaired by a coordinate transformation. The current with components

$$\begin{aligned} j_{s,x} &= D_s[(m_x + m_y) f((m_x + m_y)^2) + (m_x - m_y) f((m_x - m_y)^2)] \\ j_{s,y} &= D_s[(m_x + m_y) f((m_x + m_y)^2) - (m_x - m_y) f((m_x - m_y)^2)] \end{aligned} \tag{7.9}$$

has all the required symmetries and still has the correct physical properties. The "potentials" corresponding to Eqs. (7.6) and (7.9) are plotted in Fig. 12. Since the potential corresponding to the current (7.9) has only four discrete minima we expect "domain growth" as in spinodal decomposition, i.e., $z = 3$ and a Lifshitz-Slyozov law $r_0(t) \sim t^{1/3}$.

Siegert and Plischke[80] have numerically integrated Eq. (7.1) with periodic boundary conditions using the current (7.9) with $f(x) = (1 - x)/[(1 - x)^2 + l_d^2 x]$ both with

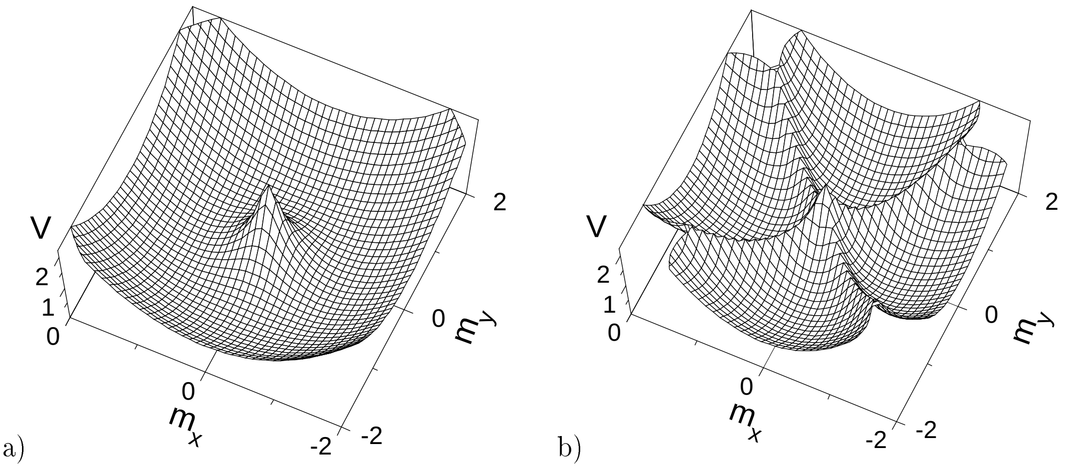

Figure 12. Potentials $V(\mathbf{m})$ correponding to the currents a) (7.6) and b) (7.9); $l_d = 10$ in both cases. Because of the size of l_d the quadratic maxima of the potentials appear very narrow.

and without noise, for a number of values of l_d. The result for the first zero $r_0(t)$ of the slope-slope correlation function for the current (7.9) is included in Fig. 11. In Fig. 13 topographic maps of the surface at an early stage of the domain growth and at the final time are shown. The square shape of the domains is clearly seen. The orientation of each of the facets is one of the four available $\{110\}$ facets. Fig. 14 shows the actual surface configurations, which correspond to the topographic maps shown in Fig. 13. The result of the numerical integration of the Langevin equation shows for a time interval of four decades (see Fig. 11) again a growth law $r_0(t) \sim t^{1/4}$. Thus, surprisingly the same result is obtained regardless of whether the form of the surface current $\mathbf{j}_s$ corresponds to the "scalar" case (7.9) or to the "vector" case (7.6). To study this problem further Eq. (7.7) was also integrated using the current (7.9) with $f = 1 - x$. The corresponding "free energy"

$$\mathcal{F} = \frac{1}{2} \int d^2x \sum_{\alpha=1}^{2} \left[(\nabla m_\alpha)^2 - m_\alpha^2 + \frac{1}{2} m_\alpha^4 \right]$$

does not couple the two components of the order parameter $\mathbf{m}$. Thus, if the two operators in front of $\mathbf{j}_s$ in Eq. (7.7) are exchanged the equation is identical to the usual Cahn-Hilliard equation for spinodal decomposition (2.19) for $d = 2$ since the two equations for the components of $\mathbf{m}$ are completely decoupled. The corresponding

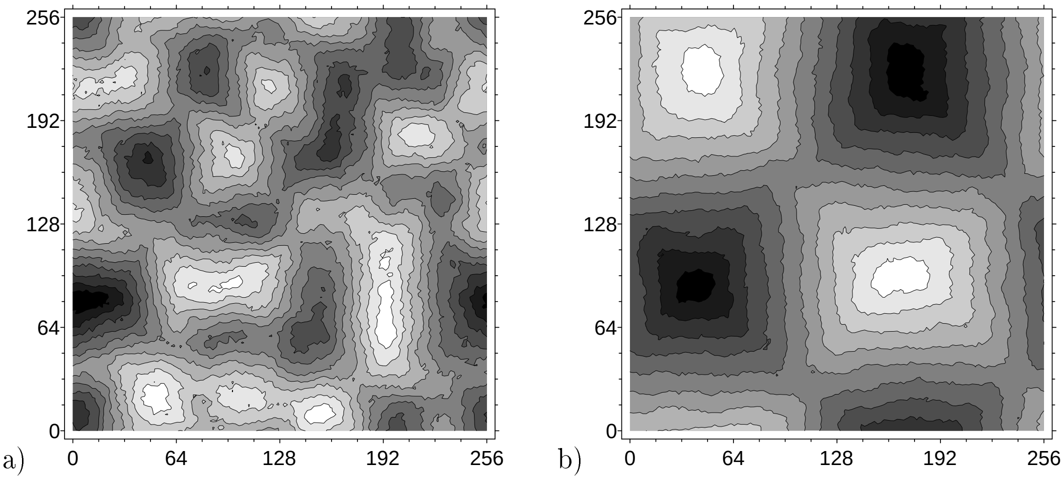

Figure 13. Contour plots of the height $h(\mathbf{r}, t)$ for the current (7.9) at a) $t = 4.65 \cdot 10^4$ and b) $t = 10^6$. Same parameters as in Fig. 11, but $\langle \eta^2 \rangle = 1$.

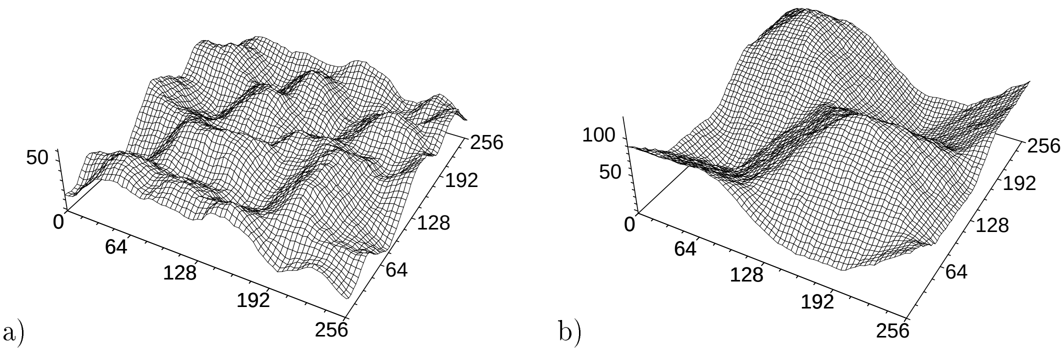

Figure 14. Surface plots corresponding to Fig. 13.

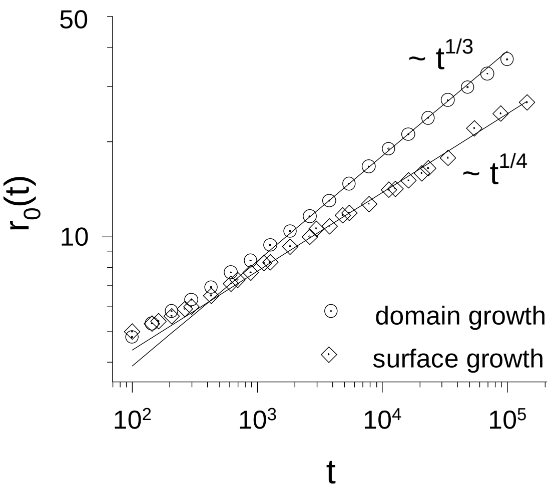

Figure 15. First zero of the slope-slope correlation function for a surface current (7.9) with $f(x) = 1 - x$. The results for the corresponding Cahn-Hilliard equation (see Fig. 5a) are included for comparison.

dynamical exponent is $z = 3$. For the present case of surface growth the two components *are coupled through the dynamics* and we again obtain $z = 4$ (see Fig. 15). We are forced to conclude that the exchange of the differential operators in front of the functional derivative of the free energy is significant, and that the constraint $\nabla \times \mathbf{m} = 0$ leads to a slower growth in comparison with the corresponding domain growth problem. Liu and Metiu[81] have integrated an equation similar to Eq. (7.7) but in a different context. Their result is in agreement with ours.

An important result of these calculations is that there is no wavelength selection in this form of the theory: In an infinite system the pyramids would continue to grow, whereas in a finite system the profile saturates when only a single pyramid remains. Instead, our theory predicts a selection of the slope, which corresponds to the order parameter in the domain growth problem. Therefore, the height and the base of the pyramids grow in the same way. Thus, we conclude that the roughness exponent ζ that characterizes the roughness of the surface in the steady state is $\zeta = 1$. This is consistent with recent experimental results[66]. The exponent $\beta = \zeta/z$ describing the growth of the pyramids is equal to $1/z$. These results follow directly from the fact that there is only *one* lengthscale and therefore only *one* exponent z in the theory of domain growth, in contrast to the conventional theories of surface roughening, which contain two independent exponents, ζ and z. It has to be emphasized, however, that these latter theories do not apply in the case of instabilities, since the surfaces are no longer self-affine and the usual scaling laws for kinetic surface roughening are not valid[73,10]. In this case, the exponents ζ and β are only effective exponents; they do not describe the scaling of, e.g., the height-height correlation functions. Furthermore, the hyperscaling relation $z = 2\zeta + d$ is not necessarily valid as has already been shown for instabilities in one dimension[10].

The theory quite naturally limits the surface roughness to $\zeta = 1$ even in the case of an instability. In $d = 1$ this roughness is in fact smaller than the one obtained for models *without* an instability[10,82,83]. These latter models are no longer consistent with the solid-on-solid assumption. Furthermore, the slope selection mechanism discussed in this section is also important if the crossover to the Kardar-Parisi-Zhang[84] universality class due to overhangs is considered. As seen in Fig. 14 basically no slopes larger than

$m = 1$ appear. Thus, overhangs are strongly suppressed and are unlikely to cause a crossover. Consequently, such a crossover can only be expected at sufficiently high temperatures, where desorption from the surface can no longer be neglected.

We predict, on the basis of the simulations, that an exponent $\beta = \zeta/z \simeq 1/4$ will be found. In a recent experiment[66] the unstable homoepitaxial growth of Cu was studied at two different temperatures and the exponent β was determined to be $\beta = 0.26$ or 0.56, at least in partial agreement with the prediction. At both temperatures the slope selection mechanism described above is observed, and consequently the roughness exponent $\zeta = 1$. More experimental and theoretical work will be needed to clarify this situation further.

SUMMARY

During the last 10 years, new theoretical approaches and numerical simulations have clarified the underlying mechanisms of phase ordering. In particular, the study of defects has proven to be very fruitful. These studies have led to a derivation of the modified Porod's law, a result for the structure factor that is independent of the dynamical details (conserved or nonconserved order parameter) of the system, but depends exclusively on the form of the defects. The energy dissipation due to defect motion allows an appealingly simple derivation of the growth laws, and furthermore, to surprising logarithmic corrections that can also be seen in simulations.

Nevertheless, several problems remain unsolved. The calculation of correlation functions for the conserved scalar order parameter is still problematic. For vector order parameters theoretical approaches to calculate the scaling functions are still missing if the dimension n is larger than the spatial dimension d, i.e., in cases where no stable localized defects exist. Numerical simulations[44] point to an exponential decay of the tail of the structure factor for $n > d$.

The important topic of the effects of quenched impurities on the growth laws has not been discussed here. In these cases the pinning of domain boundaries due to the imposed disorder leads to a slower, logarithmic growth.

The description of unstable surface growth is a challenging new problem. The similarity to ordering phenomena points to an interesting connection between theories of kinetic roughening and ordering processes, although the constraints inherent in surface growth phenomena ($\nabla \times \mathbf{m} = 0$) do not allow for a direct application of the results that have been discussed in the first sections of this article. Although the slope selection predicted by the theory has already been found in experiments, it would be desirable to obtain more experimental results for unstable growth in molecular beam epitaxy. In particular, measurements of the growth exponent z could provide further tests of the theory.

ACKNOWLEDGEMENTS

I wish to thank Michael Plischke, who introduced me to the field of kinetic roughening and with whom I enjoyed many enlightening discussions on all kinds of dynamical problems. I am very grateful to Alan Bray for numerous helpful discussions at the NATO meeting. Furthermore, I thank Michael Plischke and Joel Shore for a careful reading of the manuscript. This work was supported by the Deutsche Forschungsgemeinschaft within SFB 166.

REFERENCES

1. S. M. Allen and J. W. Cahn, Acta Metall. **27**, 1085 (1979).
2. I. M. Lifshitz, V. V. Slyozov, J. Phys. Chem. Solids **19**, 35 (1961).
3. C. Wagner, Z. Elektrochem. **65**, 581 (1961).
4. P. C. Hohenberg and B. I. Halperin, Rev. Mod. Phys. **49**, 435 (1977).
5. R. K. P. Zia, Nucl. Phys. B **251**, 676 (1985).
6. K. Kawasaki and T. Ohta, Prog. Theor. Phys. **67**, 147 (1982); **68**, 129 (1982).
7. M. Grant and J. D. Gunton, Phys. Rev. B **28**, 5496 (1983).
8. M. Siegert, Phys. Rev. A **42**, 6268 (1990).
9. R. Bausch, V. Dohm, H. K. Janssen, and R. K. P. Zia, Phys. Rev. Lett. **47**, 1837 (1981).
10. M. Siegert and M. Plischke, Phys. Rev. E **50**, Aug. 1994.
11. W. W. Mullins, J. Appl. Phys. **28**, 333 (1957); in *Metal Surfaces: Structure, Energetics and Kinetics*, Am. Soc. Metals, Metals Park, Ohio (1963), p. 17.
12. J. W. Cahn and J. E. Hilliard, J. Chem. Phys. **28**, 258 (1958); J. W. Cahn, Trans. Metall. Soc. AIME **242**, 166 (1968).
13. J. D. Gunton, M. San Miguel, and P. S. Sahni, in *Phase Transitions and Critical Phenomena*, Vol. 8, C. Domb and J. L. Lebowitz, eds., Academic Press, London (1983).
14. J. S. Langer, in *Solids far from Equilibrium*, C. Godrèche, ed., Cambridge University Press, Cambridge (1992).
15. P. Nozières, in *Solids far from Equilibrium*, C. Godrèche, ed., Cambridge University Press, Cambridge (1992).
16. D. A. Huse, Phys. Rev. B **34**, 7845 (1986).
17. J. H. Yao, K. R. Elder, H. Guo, and M. Grant, Phys. Rev. B **47**, 14110 (1993).
18. R. Bausch, R. Kree, A. Lusakowski, and L. A. Turski, Int. J. Mod. Phys. B **2**, 1537 (1988).
19. J. S. Langer and L. A. Turski, Acta Metall. **25**, 1113 (1977).
20. A. J. Bray, Phys. Rev. Lett. **62**, 2841 (1989).
21. A. J. Bray, Phys. Rev. B **41**, 6724 (1990).
22. M. Rao and A. Chakrabarti, Phys. Rev. Lett. **72**, 2911 (1994).
23. see, e.g., S.-K. Ma, *Modern Theory of Critical Phenomena*, Benjamin, Reading (1976).
24. B. I. Halperin, P. C. Hohenberg, and S.-K. Ma, Phys. Rev. Lett. **29**, 1548 (1972); Phys. Rev. B **10**, 139 (1974); Phys. Rev. B **13**, 4119 (1976).
25. A. J. Bray and A. D. Rutenberg, Phys. Rev. E **49**, R27 (1994).
26. K. Kawasaki, M. C. Yalabik, and J. D. Gunton, Phys. Rev. A **17**, 455 (1978).
27. T. Ohta, D. Jasnow, and K. Kawasaki, Phys. Rev. Lett. **49**, 1223 (1982).
28. A. J. Bray, in *Phase Transitions and Relaxation in Systems with Competing Energy Scales*, T. Riste and D. Sherington, eds., Kluwer Academic Publishers, Amsterdam (1993).
29. Y. Oono and S. Puri, Mod. Phys. Lett. B **2**, 861 (1988).
30. A. J. Bray and S. Puri, Phys. Rev. Lett. **67**, 2670 (1991).
31. A. Coniglio and M. Zannetti, Europhys. Lett. **10**, 575 (1989).
32. G. F. Mazenko, Phys. Rev. B **42**, 4487 (1990).
33. G. F. Mazenko, Phys. Rev. B **43**, 5747 (1991).
34. F. Liu and G. F. Mazenko, Phys. Rev. B **45**, 6989 (1992).
35. A. J. Bray and K. Humayun, J. Phys. A **25**, 2191 (1992).
36. A. J. Bray and K. Humayun, Phys. Rev. Lett. **68**, 1559 (1992).
37. M. Abramowitz and I. A. Stegun, eds., *Handbook of Mathematical Functions*, Dover, New York (1970).
38. I. S. Gradshteyn and I. M. Ryzhik, *Tables of Integrals, Series, and Products*, Academic Press, San Diego (1980).
39. A. J. Bray, Phys. Rev. E **47**, 228 (1993).
40. C. Yeung, Y. Oono, and A. Shinozaki, Phys. Rev. E **49**, 2693 (1994).
41. G. Porod, Kolloid Z. **124**, 83 (1951); **125**, 51 (1952).
42. H. Toyoki, Phys. Rev. B **45**, 1965 (1992).
43. G. F. Mazenko, O. T. Valls, and M. Zannetti, Phys. Rev. B **38**, 520 (1992).
44. M. Rao and A. Chakrabarti, Phys. Rev. E **49**, 3727 (1994).
45. M. Mondello and N. Goldenfeld, Phys. Rev. E **47**, 2384 (1993).
46. J. G. Amar, F. E. Sullivan, and R. D. Mountain, Phys. Rev. B **37**, 196 (1988).
47. C. Roland and M. Grant, Phys. Rev. B **39**, 11971 (1989).
48. A. J. Bray and K. Humayun, J. Phys. A **23**, 5897 (1990).
49. R. Rajaraman, *Solitons and Instantons*, North-Holland, Amsterdam (1982).

50. M. Mondello and N. Goldenfeld, Phys. Rev. A **42**, 4514 (1990).
51. M. Mondello and N. Goldenfeld, Phys. Rev. A **45**, 657 (1992).
52. H. Toyoki, J. Phys. Soc. Jpn. **60**, 1433 (1991).
53. H. Toyoki, J. Phys. Soc. Jpn. **60**, 1153 (1991).
54. M. Grant, M. San Miguel, J. Viñals, and J. D. Gunton, Phys. Rev. B **31**, 3027 (1985).
55. T. M. Rogers, K. R. Elder, and R. C. Desai, Phys. Rev. B **37**, 9638 (1988).
56. Y. Oono and S. Puri, Phys. Rev. Lett. **58**, 836 (1987); Phys. Rev. A **38**, 434 (1988); S. Puri and Y. Oono, *ibid.* **38**, 1542 (1988).
57. W. H. Press, S. A. Teukolsky, W. T. Vetterling, and B. P. Flannery, *Numerical Recipes*, Cambridge University Press, Cambridge (1992), chap. 19.
58. M. Siegert and M. Rao, Phys. Rev. Lett. **70**, 1956 (1993).
59. R. Toral, A. Chakrabarti, and J. D. Gunton, Phys. Rev. Lett. **60**, 2311 (1988); A. Chakrabarti, R. Toral, and J. D. Gunton, Phys. Rev. B **39**, 4386 (1989).
60. T. M. Rogers and R. C. Desai, Phys. Rev. B **39**, 11956 (1989).
61. A. Coniglio, Y. Oono, A. Shinozaki, and M. Zannetti, Europhys. Lett. **18**, 59 (1992).
62. J. Villain, J. Phys. I (France) **1**, 19 (1991).
63. G. Ehrlich and F.G. Hudda, J. Chem. Phys. **44**, 1039 (1966); S. C. Wang and G. Ehrlich, Phys. Rev. Lett. **70**, 41 (1993).
64. R. L. Schwoebel and E. J. Shipsey, J. Appl. Phys. **37**, 3682 (1966); R. L. Schwoebel, J. Appl. Phys. **40**, 614 (1969).
65. M. Bott, T. Michely, G. Comsa, Surf. Sci. **272**, 161 (1992).
66. H.-J. Ernst, F. Fabre, R. Folkerts, and J. Lapujoulade, Phys. Rev. Lett. **72**, 112 (1994).
67. M. D. Johnson, C. Orme, A. W. Hunt, D. Graf, J. Sudijono, L. M. Sander, and B. G. Orr, Phys. Rev. Lett. **72**, 116 (1994).
68. S. F. Edwards and D. R. Wilkinson, Proc. Roy. Soc. (London), A **381**, 17 (1982).
69. D. E. Wolf, private communication.
70. S. Stoyanov and D. Kashchiev, in *Current Topics in Materials Science*, Vol. 7, edited by E. Kaldis, North Holland, Amsterdam (1981); J. A. Venables, G. D. Spiller, and M. Hanbücken, Rep. Prog. Phys. **47**, 399 (1994); J. Villain, A. Pimpinelli, L.-H. Tang, and D. E. Wolf, J. Phys. I (France) **2**, 2107 (1992); J. Villain, A. Pimpinelli, and D. E. Wolf, Comments Cond. Mat. Phys. **16**, 1 (1992).
71. D. E. Wolf, talk given at the workshop *Surface Phase Transitions*, Trieste (1991).
72. G. S. Bales and A. Zangwill, Phys. Rev. B **41**, 5500 (1990).
73. M. Siegert and M. Plischke, Phys. Rev. Lett. **68**, 2035 (1992).
74. J. Krug, M. Plischke, and M. Siegert, Phys. Rev. Lett. **70**, 3271 (1993).
75. T. Kawakatsu and T. Munakata, Prog. Theor. Phys. **74**, 11 (1985).
76. P. Smilauer, M. R. Wilby, and D. D. Vvedensky, Phys. Rev. B **47**, 4119 (1993).
77. D. D. Vvedensky, A. Zangwill, C. N. Luse, and M. R. Wilby, Phys. Rev. E **48**, 852 (1993).
78. A. W. Hunt, C. Orme, D. R. M. Williams, B. G. Orr, and L. M. Sander, this Volume.
79. I. Elkinani and J. Villain, Solid State Comm. **87**, 105 (1993); J. Phys. I (France) **4**, 949 (1994).
80. M. Siegert and M. Plischke, preprint Mar. 1994, submitted to Phys. Rev. Lett.
81. F. Liu and H. Metiu, Phys. Rev. B **48**, 5808 (1993).
82. D. E. Wolf and J. Villain, Europhys. Lett. **13**, 389 (1990).
83. J. G. Amar, P.-M. Lam, and F. Family, Phys. Rev. E **47**, 3242 (1993).
84. M. Kardar, G. Parisi, and Y.-C. Zhang, Phys. Rev. Lett. **56**,889 (1986).